Biomedicine & Pharmacotherapy 178 (2024) 117259

Contents lists available at ScienceDirect

Biomedicine & Pharmacotherapy

journal homepage: www.elsevier.com/locate/biopha

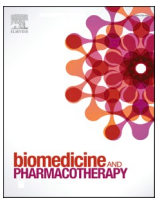

Induced pluripotent stem cell-derived mesenchymal stem cells reverse bleomycin-induced pulmonary fibrosis and related lung stiffness

Amlan Chakraborty [a,b,1], Chao Wang [a,1], Margeaux Hodgson-Garms [c], Brad R.S. Broughton [a], Jessica E. Frith [c], Kilian Kelly [d], Chrishan S. Samuel [a,e,*]

[a] Cardiovascular Disease Program, Monash Biomedicine Discovery Institute (BDI) and Department of Pharmacology, Monash University, Clayton, Victoria, Australia
[b] Division of Immunology, Immunity to Infection and Respiratory Medicine, The University of Manchester, Manchester, England, UK
[c] Department of Materials Science and Engineering, Monash University, Clayton, Victoria, Australia
[d] Cynata Therapeutics Ltd, Cremorne, Victoria, Australia
[e] Department of Biochemistry and Pharmacology, The University of Melbourne, Parkville, Victoria, Australia

ARTICLE INFO

Keywords:
Pulmonary fibrosis
Tissue remodelling
Stem cell therapy
iPSC-derived MSCs

ABSTRACT

Idiopathic pulmonary fibrosis (IPF) is characterised by lung scarring and stiffening, for which there is no effective cure. Based on the immunomodulatory and anti-fibrotic effects of induced pluripotent stem cell (iPSC) and mesenchymoangioblast-derived mesenchymal stem cells (iPSCs-MSCs), this study evaluated the therapeutic effects of iPSCs-MSCs in a bleomycin (BLM)-induced model of pulmonary fibrosis. Adult male C57BL/6 mice received a double administration of BLM (0.15 mg/day) 7-days apart and were then maintained for a further 28-days (until day-35), whilst control mice were administered saline 7-days apart and maintained for the same time-period. Sub-groups of BLM-injured mice were intravenously-injected with 1×10^6 iPSC-MSCs on day-21 alone or on day-21 and day-28 and left until day-35 post-injury. Measures of lung inflammation, fibrosis and compliance were then evaluated. BLM-injured mice presented with lung inflammation characterised by increased immune cell infiltration and increased pro-inflammatory cytokine expression, epithelial damage, lung transforming growth factor (TGF)-β1 activity, myofibroblast differentiation, interstitial collagen fibre deposition and topology (fibrosis), in conjunction with reduced matrix metalloproteinase (MMP)-to-tissue inhibitor of metalloproteinase (TIMP) ratios and dynamic lung compliance. All these measures were ameliorated by a single or once-weekly intravenous-administration of iPSC-MSCs, with the latter reducing dendritic cell infiltration and lung epithelial damage, whilst promoting anti-inflammatory interleukin (IL)-10 levels to a greater extent. Proteomic profiling of the conditioned media of cultured iPSC-MSCs that were stimulated with TNF-α and IFN-γ, revealed that these stem cells secreted protein levels of immunosuppressive factors that contributed to the anti-fibrotic and therapeutic potential of iPSCs-MSCs as a novel treatment option for IPF.

Abbreviations: AAD, allergic airways disease; BALF, bronchoalveolar lavage fluid; BLM, bleomycin; BM, basement membrane; CART, collagen area to tissue ratio; CCL2, chemokine C-C motif ligand 2; CCR4, chemokine receptor type 4; CD, cluster of differentiation; CM, conditioned media; DC, dendritic cell; DMEM-LG, Dulbecco's Modified Eagle Medium with low glucose; ERK, extracellular signal-regulated kinase; FBS, fetal bovine serum; H&E, haematoxylin and eosin; IDO1, indoleamine 2,3-dioxygenase 1; IL, interleukin; IFN, interferon; IPF, idiopathic pulmonary fibrosis; iPSC, induced pluripotent stem cell; JNK, c-Jun N-terminal kinase; LC-MS/MS, liquid chromatography tandem mass spectrometry; LFQ, label free quantification; MAP, mitogen-activated protein; MMP, matrix metalloproteinase; MSC, mesenchymal stem cell; PGE2, prostaglandin E2; PTGES3, prostaglandin E synthase 3; RANTES, regulated upon activation, normal T cell expressed and presumably secreted; SHG, second harmonics generation; Smad, suppressor of mothers against decapentaplegic; TIMP, tissue inhibitor of metalloproteinase; TNF, tumour necrosis factor; TPE, two-photon excitation fluorescence; TSG-6, tumor necrosis factor-α-stimulated gene 6; Treg, regulatory T cells; VEGF, vascular endothelial growth factor.

* Correspondence to: Cardiovascular Disease Program, Monash Biomedicine Discovery Institute and Department of Pharmacology, Monash University, Clayton, Victoria, Australia.
E-mail address: chrishan.samuel@monash.edu (C.S. Samuel).
[1] These authors contributed equally to the study

https://doi.org/10.1016/j.biopha.2024.117259
Received 3 June 2024; Received in revised form 23 July 2024; Accepted 2 August 2024
Available online 7 August 2024

1. Introduction

Idiopathic pulmonary fibrosis (IPF) is a chronic interstitial lung disease characterised by aberrant tissue remodelling-induced scarring of the lungs and an irreversible decline in lung function [1,2]. Whilst the aetiology of IPF is not well understood, it is classified as a multifactorial disorder associated with several risk factors such as aging, sex, genetic predisposition and smoking [3,4]. IPF is considered a rare disease, although its incidence can vary significantly according to geographical location [5]. Its annual incidence is estimated at 16.3–17.4 cases in the United States, 0.22–7.4 cases in Europe [5] and 10.4–11.2 cases in Australia [6] per 100,000 people; which is expected to increase globally over time. Despite its low incidence, IPF is associated with high mortality rates that result from respiratory failure within 3–5 years of diagnosis [7], and hence, is a significant healthcare concern.

Despite these alarming statistics, there are currently no effective therapies for IPF that can completely halt or reverse disease progression. When IPF was initially defined as a chronic inflammatory disorder, traditional anti-inflammatory or immunosuppressive medications were used to treat the disease, but were largely ineffective [8,9]. As inflammation is now regarded as a secondary contributor to disease pathogenesis, anti-fibrotic agents such as pirfenidone and nintedanib (which block the pro-fibrotic actions of specific growth factors that promote fibrogenesis), are now used as frontline treatments for IPF [10–14]. However, pirfenidone only slows down disease progression as it does not reverse established disease pathology, and is associated with various adverse effects including photosensitivity and GI disturbances [10,11,15,16]. Hence, there is an urgent need for an alternative therapeutic option that can particularly regress established disease pathology.

Mesenchymal stem cells (MSCs) are self-renewing, multipotent stromal cells that have the capacity to divide into a few cell lineages, but also possess immunomodulatory, anti-remodelling and tissue-reparative properties as a stem cell therapy [17]. These cells are immunoprivileged as they express class I major histocompatibility complex but lack class II major histocompatibility complex and costimulatory molecules CD80, CD86, and CD40 [18,19]. MSCs also home to the injured tissue through the expression of the chemokine receptor type 4 (CCR4) [20]. However, there are certain limitations to the therapeutic application of MSCs in that they have not consistently relieved the adverse symptoms associated with chronic disease settings; the outcomes of MSC treatment can vary depending on their tissue origin/source, extent of culture expansion, donor-dependent viability and efficacy, and the timing of their administration; and only a relatively small number of MSCs can be isolated from each donor organ [21–23].

To overcome these limitations, Cynata Therapeutics have used Cymerus™ technology to differentiate human induced pluripotent stem cells (iPSCs) into precursor cells known as mesenchymoangioblasts (a class of early clonal mesoendodermal precursor cells) and subsequently into MSCs (iPSC-derived MSCs; iPSC-MSCs) [24]. As iPSCs can proliferate indefinitely and because mesenchymoangioblasts can expand into extremely large quantities of MSCs, sufficient iPSC-MSCs can be acquired from a single master cell bank of iPSCs derived from a single healthy blood donor (limiting donor- and expansion-dependent variability and contamination from nontarget cells) without the need for excessive culture expansion once MSCs are formed. Furthermore, these iPSC-MSCs were found to home to the inflamed lungs of mice with established chronic allergic airways disease (AAD) for up to 5 days post-administration [25], and effectively reduced airway inflammation, subepithelial airway fibrosis and airway hyperresponsiveness independently of their delivery route [26]; the latter two measures to a greater extent than corticosteroid treatment [25]. Not only did these iPSC-MSCs attenuate myofibroblast-induced fibrogenesis within the airways, they also promoted the expression levels of collagen-degrading matrix metalloproteinases (MMPs) that can facilitate the breakdown of established fibrosis.

Hence, in this study, we determined the cellular mechanisms and downstream targets by which these iPSC-MSCs acted through to reverse established interstitial lung fibrosis and related collagen topology and lung stiffness in a preclinical model of bleomycin (BLM)-induced lung injury, the most characterised and widely-used model of pulmonary fibrosis [27]. Proteomic profiling of the condition media of cultured iPSC-MSCs was also performed to further evaluate the immunomodulatory effects of these stem cells.

2. Materials and methods

2.1. Materials

Bleomycin sulfate (BLM) was obtained from Cayman Chemical (catalogue number: 9041–93–4; Ann Arbor, MI, USA). iPSC-MSCs were provided by Cynata Therapeutics Ltd.

2.2. Animals

10–12 week-old male C57BL/6 J mice, weighing approximately 25–30 g were obtained from Monash Animal Services (Monash University, Clayton, VIC, Australia) and used to determine if a single (x1) or double/once-weekly (x2) administration of iPSC-MSCs could reduce established BLM-induced interstitial lung fibrosis and related stiffness; and evaluate the mechanisms of action involved. All mice were housed (in groups of three to four mice per cage) under a controlled environment, given a 5- to 6-day acclimatisation period before they were subjected to any experimentation, and maintained on a 12-h light/12-h dark cycle with free access to normal rodent lab chow (Barastock Stockfeeds, Pakenham, VIC, Australia) and water. All animal care and experimental procedures performed were approved by an Animal Ethics Committee of Monash University (under animal ethics number: MARP/2020/23529), which adheres to the guidelines for the Care and Use of Laboratory Animals for Scientific Purposes (National Health and Medical Research Council, Canberra, ACT, Australia). Male mice were used as they are more prone to BLM-induced lung inflammation and fibrosis compared to their age-matched female counterparts [28,29]; hence, male mice presented a larger therapeutic window in which the anti-inflammatory and anti-fibrotic effects of iPSC-MSCs could be determined.

2.3. Induction and treatment of BLM-induced pulmonary fibrosis

Male C57BL/6 J mice (n=30) were intranasally (i.n)-administered bleomycin sulphate (BLM) on Days-0 and -7 (0.15 mg in 50 μl of saline (SAL); 25 μl per nare on each day) [30], then left for a further four-weeks for lung inflammation and fibrosis to develop. One sub-group of BLM-injured mice were left untreated until day-35 post-injury (injury control group; n=10). A second sub-group of BLM-injured mice were given a single tail vein injection of 1×10^6 iPSC-MSCs on day-21 post-injury, then maintained until day-35 post-injury (iPSC-MSC x1 treated group; n=10). A third sub-group of BLM-injured mice were given a tail vein of 1×10^6 iPSC-MSCs on day-21 and day-28 post-injury, then maintained until day-35 post-injury (iPSC-MSC x2 treated group; n=10). The dose of iPSC-MSCs used in this study was based on our previous findings [26], in which the once-weekly i.v-administration of 1×10^6 iPSC-MSCs to mice subjected to 9-weeks of chronic AAD, at the beginning of week-10 and week-11, therapeutically reduced several measures of airway/lung remodelling, fibrosis and dysfunction in the absence of any adverse effects on animal mortality. A further control group of mice were i.n-administered 50 μl of SAL on Days-0 and -7 (25 μl per nare on each day), and maintained until day-35 (healthy control group; n=10).

iPSC-MSCs were supplied in bags containing 1×10^8 cells in each bag. These bags were shipped to Monash University in liquid nitrogen and stored at −80°C (for 5–7 days at most) before use. On each day of iPSC-MSC injection into respective mice, each bag was thawed at 37 °C, before the 1×10^8 million cells in each bag were washed twice in warmed sterile phosphate buffered saline (PBS), and reconstituted in 20 ml of

warmed PBS. Of this 20 ml PBS solution containing cells, 200μl (containing 1×10^6 cells) were delivered to each mouse at the appropriate time-point via a tail vein injection. Notably, an intravenous (i.v) injection was used as it is a clinically-feasible route of cell delivery; and the lung is the major site of cell migration following an i.v injection [31].

Initially, groups of equal size (n=10 per group) were designed using randomization and blinded analysis. However, to account for the possibility that some mice might fail to tolerate BLM and/or iPSC-MSC administration, power calculations were performed to ensure that adequate group sizes were used for the studies detailed below, where it was determined that with a 25 % SD, we would be 80 % powered to detect a 20–30 % effect with n = 6–10 animals per group.

2.4. Evaluation of dynamic lung compliance

On day 35 post-(the first) BLM or SAL administration to mice, all mice were evaluated by plethysmography for changes in dynamic lung compliance [32,33]. Mice were briefly anesthetized with an i.p. injection of ketamine (100 mg/kg body weight) and xylazine (20 mg/kg body weight), tracheostomized and cannulated. As bronchial smooth muscle contraction has been found to significantly influence lung compliance [34], increasing doses of methacholine (0-50 mg/ml) were nebulized for dynamic compliance to be measured (Biosystem XA version 2.7.9, Buxco Electronics, Troy, NY, USA) for 2 minutes after each dose of methacholine. The results were expressed as the percentage change in dynamic compliance after each dose of methacholine from baseline compliance. To then better illustrate changes in dynamic compliance between the various treatment groups investigated, the respective % change in dynamic compliance that was subtracted from each respective baseline value in response to the highest dose of methacholine tested (50 mg/ml) was presented.

2.5. Bronchoalveolar lavage fluid and tissue collection

Once dynamic lung measurements were completed and whilst mice were still anaesthetised, bronchoalveolar lavage fluid (BALF) was extracted from mice as outlined previously [35], by infusing and removing three 1 ml washes of ice-cold saline, which were pooled for flow cytometry analysis of immune cell subsets. Following BALF collection, mice were culled with an overdose of anaesthetic containing ketamine and xylazine, before their lung tissue isolated. The lungs of each animal were then divided along the transverse plane, resulting in four separate lobes. In each case, the largest lung lobe was fixed in 10 % neutral buffered formalin overnight and processed to be cut and embedded in paraffin wax. The remaining lobes were separately snap-frozen in liquid nitrogen and eventually stored at -80^0 C for various other assays.

2.6. Flow cytometry analysis of the BALF

Cells isolated from the BALF were counted and the concentration adjusted to 1×10^5 cells/ml in a 50 μl volume for staining and fluorescence-activated cell sorting (FACS) analysis. A rat anti-mouse Fc block (CD16/CD32; #553141; 1:50 dilution; Becton Dickinson (BD) Horizon, Franklin Lakes, NJ, USA) was applied to cells from all control and treatment groups to minimize nonspecific Fc binding. Subsequently, cells were stained in FACS buffer (dPBS+2 % HI-FCS) using the following anti-mouse antibodies: CD11c-BUV395 (#564080; 1:100 dilution; BD Horizon); CD45-PE-Cy5 (#553082; 1:200 dilution; BD Biosciences, San Jose, CA, USA); F4/80-APC-Fire750 (#123151; 1:100 dilution; BioLegend, San Diego, CA, USA); CD206-AF647 (#141711; 1:100 dilution; BioLegend); CD4-BUV496 (#741050; 1:200 dilution; BD Biosciences); CD25-BV785 (#564368; 1:100 dilution; BD Biosciences); FoxP3-BV421 (#561293; 1:100 dilution; BD Biosciences). Live/dead staining was conducted using zombie dye (#423101; 1:1000 dilution; BioLegend), excluding unstained and fluorescent minus one (FMO) controls.

Following primary antibody staining (with the exception of FoxP3) and live/dead cell staining, intra-cellular staining for FoxP3 was performed using FoxP3/Transcription Factor Staining Buffer Set (#00–5523; Affymetrix eBioscience; Santa Clara, CA, USA). Fresh FoxP3 fixation/permeabilization working solution was prepared in a 1:3 concentrate with diluent along with permeabilization buffer in a 1:9 ratio with distilled water. Following the final wash after primary cell staining, the supernatant was discarded before 200μl of FoxP3 fixation/permeabilization working solution was added to the cell pellet. Samples were incubated for 1 hour at room temperature in the dark, then centrifuged at 500 g for 5 minutes at room temperature before the supernatants were discarded. 200μl of 1x permeabilization buffer was added to resuspend the cells. This cell resuspension procedure was repeated twice before cell pellets were finally resuspending in 100μl of permeabilization buffer containing the anti-mouse Foxp3-BV421 antibody, which was left to incubate in the dark for 1 hour at room temperature. The cells were then washed twice with 200μl of 1x permeabilization buffer by centrifugation. Cells were resuspended in FACS buffer and washed once followed by fixing the cells with dPBS+1 % PFA. Data was acquired using a BD Fortessa Flow Cytometer x20; which was housed at the Monash FlowCore Platform (Clayton, Victoria, Australia).

Unstained cells were utilized to set voltages for Forward Scatter (FSC) and Side Scatter (SSC), followed by acquisition of the single-cell control using compensation beads (ABC compensation beads; #A10497; Invitrogen/Thermo Fisher Scientific; Scoresby, Victoria, Australia). Data acquisition was performed using BD FACS Diva and analysed with FlowJo. Firstly, all cells were gated based on their size and granularity using FSC-A/SSC-A followed by doublet exclusion using FSC-A/FSC-H to get single cells. Zombie/SSC-A was used to negatively select cells which were live. Macrophages were gated as $CD45^+$ and M2-skewed macrophages were $F4/80^+CD206^+$. Dendritic cells were gated as $CD11c^+$ cells and regulatory T cells were gated first by selecting Th cells as $CD4^+$ and then $CD25^{Hi}FoxP3^+$ cells. Although additional gating for DCs could have been performed, previous studies had confirmed that $CD11c^+$ is considered a reliable marker of DCs *in vivo* [36] and often used to identify DCs in the murine lung [37,38]. The same gating strategy was applied to all replicates from control as well as treatment groups. FMOs were used to properly place the gates for CD45 and CD11c. A separate FMO was used to control for non-specific FoxP3 binding.

2.7. ELISA analysis of BALF cytokine levels

Total protein was measured from the BALF using the BioRad Protein Assay Dye (BioRad Laboratories, Granville, NSW, Australia), for the assessment of pro-inflammatory markers: TNF-α, IL-1β and IL-6; and anti-inflammatory markers: IL-10 and IFN-γ. In each case, equivalent protein from each sample was assayed using Quantikine ELISA kits for either mouse TNF-α (RDSMTA00B; 1:1000 dilution), mouse IL-1β/IL-1F2 (RDSMLB00C; 1:1000 dilution), mouse IL-6 (RDSM6000B; 1:1000 dilution); mouse IL-10 (RDSM1000B; 1:1000 dilution) or mouse IFN-γ (RDSMIF00; 1:1000 dilution) (all from R&D Systems, Minneapolis, MN, USA). Assays were performed in duplicate according to manufacturer's instructions, against serially-diluted standards.

2.8. Histology and immunohistochemistry

Formalin-fixed, paraffin-embedded lung tissue (from the largest lung lobe of each mouse) was cut into 4μm serial sections. One serial section from each animal was stained with haematoxylin and eosin (H&E) for the assessment of inflammatory cell infiltration and changes in lung architecture. A separate serial section from each animal was stained with Masson's trichrome to visualise interstitial lung fibrosis. Separate serial paraffin-embedded sections were used to assess the localization of

thymic stromal lymphopoietin (TSLP; a marker of epithelial damage [33], which is expressed by alveolar epithelial cells in IPF patients and BLM- injured mice [39,40]), the pro-fibrotic cytokine, TGF-β1, and α-SMA (as a marker of myofibroblast differentiation). All sections were subjected to antigen retrieval in a sodium citrate buffer, treated with antibody diluent (Dako, North Sydney, NSW, Australia) to block non-specific immunoreactivity, and then incubated overnight with rabbit polyclonal (IgG) antibodies to detect either TSLP (ABT330; EMD Millipore Corporation, Temcula, CA, USA) or TGF-β1 (#ab92486, 1:250 dilution; Abcam Antibodies), or a mouse monoclonal (IgG2a) antibody, clone 1A4 to detect α-SMA (#M0851, 1:500, Dako). The following day, all sections were stained with either a Dako Envision + streptavidin-HRP (HRP)-labelled polymer anti-mouse (IgG) secondary antibody (#E0464; Agilent Technologies, Mulgrave, VIC, Australia) for the detection of α-SMA (Dako); or HRP-labelled polymer anti-rabbit IgG secondary antibody (for the detection of TGF-β1; Dako). Binding was visualised by 3,30 -diaminobenzidine (Dako), before slides were counterstained with haematoxylin and mounted in DePex (VWR International, Radnor, PA, USA). In each case, additional sections that were not stained with the above-mentioned primary antibodies were included to ensure antibody specificity. All histological and immunohistochemical-stained slides were scanned and captured with the Aperio Scanscope AT Turbo scanner (Leica Biosystems, Nussloch, Germany) and assessed with ImageJ 1.48 software (NIH, Bethesda, MD, USA) in a blinded fashion. In each case, semi-quantification (of lung inflammation, interstitial lung fibrosis, interstitial lung myofibroblast accumulation and interstitial lung TGF-β1 expression) was performed on eight to 10 consecutive non-overlapping fields per lung section analysed, which were randomly selected and analysed at x400 magnification. Inflammatory cell infiltration was semi-quantitated in a blinded fashion from H&E-stained slides using a 0–4 scoring system described previously [32]; where 0 = no visible inflammation; 1 = occasional inflammatory cell aggregates, pooled size $<0.1\,mm^2$; 2 = some inflammatory cell aggregates, pooled size of $0.2\,mm^2$; 3 = widespread inflammatory cell aggregates, pooled size of $0.3\,mm^2$; 4 = extensive inflammatory infiltration, pooled size of $0.6\,mm^2$. Epithelial damage was analysed by counting the number of TSLP-stained cells within the lung epithelium; which was expressed as the number of cells per 100 μm of basement membrane (BM) length. Interstitial lung fibrosis was determined by measuring the blue stained extracellular matrix deposition from Masson's trichrome-stained sections; and expressing the data as the % fractional area per field analysed. Interstitial lung myofibroblast accumulation was quantified by measuring the α-SMA (brown)-stained myofibroblast accumulation; and expressed as the % myofibroblast staining per field analysed. Interstitial lung TGF-β1 staining was quantified by measuring the levels of strong positively stained (brown) areas within the interstitial regions, respectively; and expressing the data as the % interstitial TGF-β1 staining per field analysed.

2.9. HistoIndex analysis of interstitial collagen topology

To assess changes in interstitial lung collagen topology from the various treatment groups established, a separate serial section from the largest lung lobe was assessed using the stain-free, second harmonics generation (SHG)-based HistoIndex platform, as outlined previously [41]. Following the optimisation protocol and the scanning of lung tissue sections to acquire SHG (green) and two-photon excitation fluorescence (red) signals from each section, the FibroIndex software was then used to assess changes in interstitial lung collagen area to tissue ratio (CART), interstitial collagen fiber density and thickness, interstitial collagen fiber length and interstitial collagen fiber counts [41].

2.10. Western blotting

Equivalent amounts of lung protein (from the second largest lung lobe of each mouse; 10–15 μg per sample) were run on 4–15 % SDS-PAGE gels and analysed by Western blotting [42,43]. As TGF-β1 is recognised as the major pro-fibrotic cytokine that is stimulated by BLM to promoting lung fibrosis [44,45], changes in intracellular proteins that regulate TGF-β1 signal transduction were evaluated. Changes in canonical Smad2 phosphorylation (pSmad2) and pSmad3 (which promote TGF-β1 signal transduction) and Smad7 (which inhibits TGF-β1 signal transduction) were assessed using rabbit monoclonal (IgG) antibodies to detect either pSmad2 (only when dually phosphorylated at serines 465 and 467; #3108; 1:1000 dilution; Cell Signaling Technology, Danvers, MA, USA) or pSmad3 (only when dually phosphorylated at serines 465 and 467; #9520; 1:1000 dilution; Cell Signaling Technology); or a rabbit polyclonal (IgG) antibody to detect Smad7 (ab216428; 1:1000 dilution; Abcam Antibodies, Cambridge, MA, USA). Changes in non-canonical mitogen-activated protein (MAP) kinase (MAPK) activity were assessed using rabbit polyclonal (IgG) antibodies to detect either pERK1/2 (when phosphorylated either individually or dually at threonine 202 and tyrosine 204 of ERK1; #9101; 1:1000 dilution; Cell Signaling Technology); pJNK (when dually phosphorylated at threonine 183 and tyrosine 185; #9251; Cell Signaling Technology); or pp38 MAPK (only when activated by phosphorylation at threonine 180 and tyrosine 182; #9211; 1:1000 dilution; Cell Signal Technology). Membranes probed for pSmad2 or pSmad3 were reprobed with a polyclonal (IgG) antibody to detect total Smad2/3 (#3102; 1:1000 dilution; Cell Signaling Technology), to confirm the equivalent loading of protein samples. Similarly, membranes probed for pERK1/2 were reprobed with a monoclonal (IgG1) antibody to detect total ERK1/2 (#4696; 1:1000 dilution; Cell Signaling Technology). On the other hand, membranes probed for pJNK were also probed with a polyclonal antibody to detect total p38 MAPK (#9212; 1:1000 dilution; Cell Signaling Technology), then reprobed with either a polyclonal antibody to detect total JNK (#9252; 1:1000 dilution; Cell Signaling Technology) or the antibody to detect pp38 MAPK. Membranes probed for Smad7 were reprobed with a rabbit monoclonal (IgG) antibody to detect GAPDH (clone 14C10; #2118; 1:2000 dilution; Cell Signaling Technology).

As sub-groups of matrix metalloproteinases (MMPs), such as collagenases, can degrade collagen when activated, changes in lung MMP-13 (collagenase 3; the primary collagenase in mice) were detected using a monoclonal (IgG1) antibody to MMP-13 (MA5–14238; 1:1000 dilution; Thermo Fisher Scientific). As MMP activity can be inhibited by tissue inhibitor of metalloproteinase (TIMP) activity, changes in lung TIMP-1 and TIMP-2 were also detected using or a polyclonal (IgG) antibody to TIMP-1 (ab38978; 1:1000 dilution; Abcam Antibodies) or rabbit monoclonal (IgG) antibody to TIMP-2 (#5738; 1:1000 dilution; Cell Signaling Technology). In each case, these membranes were reprobed with a rabbit monoclonal (IgG) antibody to detect GAPDH (Cell Signaling Technology), to confirm the equivalent loading of protein samples. In all cases, membranes were further probed with a goat anti-rabbit HRP (#7074; 1:2000 dilution; Cell Signaling Technology) or horse anti-mouse HRP (#7076; 1:2000 dilution; Cell Signaling Technology) IgG secondary antibodies, respectively. Proteins were then detected using the Clarity Western ECL substrate detection kit and quantified by densitometry with a ChemiDoc MP Imaging System and Image Lab v.6.0 software (both from Bio-Rad Laboratories, Hercules, CA, USA) [42,43]. The densitometry values were then expressed relative to the value from the saline-treated control group, which was expressed as 1 in each case. Representative blots of the appropriate end points determined were also chosen for presentation in each case.

2.11. Gelatin zymography

Equivalent amounts of lung protein (5–10μg per sample) were additionally analysed on SDS-PAGE gels consisting of 7.5 % acrylamide and 1 mg/ml gelatin, to assess changes in MMP-2 (gelatinase A) and MMP-9 (gelatinase B) levels from all groups studied, as detailed previously [43,46]. Gelatinases can further degrade collagenase-digested collagen into gelatin, and gelatinolytic activity was indicated by clear

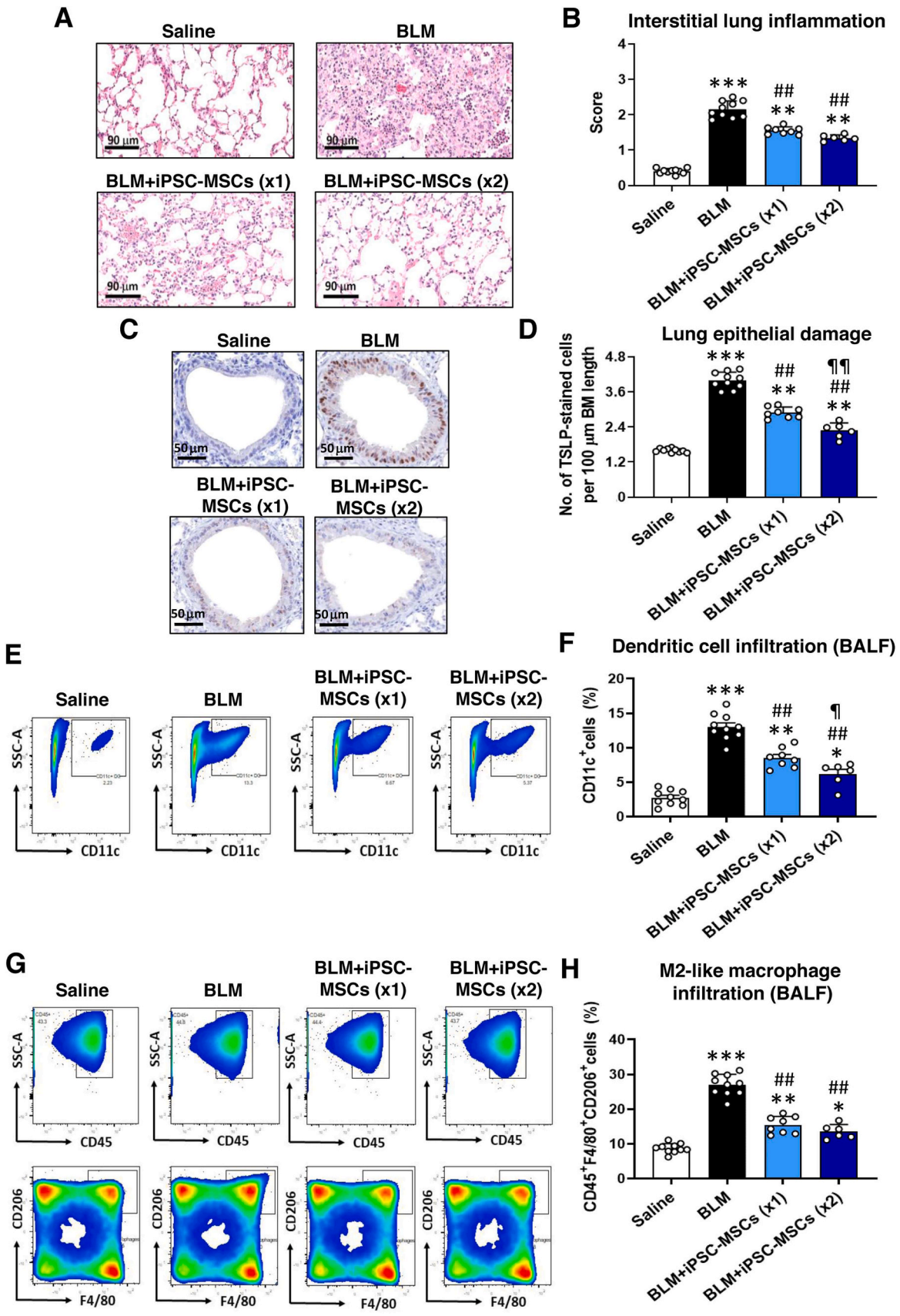

(caption on next page)

Fig. 1. Cynata™-iPSC-MSC-treatment of BLM-injured mice ameliorated measures of lung inflammation, epithelial damage and inflammatory cell infiltration into the BALF. (A,C) Representative H&E- (A) and TSLP (brown)- (C) stained images (at x400 magnification) show the extent of inflammatory cell infiltration within the lung and TSLP-associated lung epithelial damage, respectively, in each of the groups investigated. Scale bar = 90 μm (A) or 50 μm (C). (E,G) Representative flow cytometry plots from the BALF samples of each the groups evaluated, show the expression of $CD11c^+$ dendritic cells (E) or separation of myeloid cell subsets according to $CD45^+F4/80^+CD206^+$ (M2-like macrophage) expression (G). All gating was performed on fluorescent-minus-one (FMO) controls and unstained cells. (B,D, F,H) Also shown are the mean ± SEM interstitial lung inflammation score (from 10 non-overlapping fields of view per lung section analysed) (B); number (No.) of TSLP-stained cell per 100 μm basement membrane (BM) length (from 10 non-overlapping fields of view per lung section analysed) (D); % $CD11c^+$ cells within the BALF (F) or % $CD45^+F4/80^+CD206^+$ cells within the BALF (H) from n=6–10 mice per group. $^*P < 0.05$, $^{**}P < 0.01$, $^{***}P < 0.001$ versus the saline-instilled control group; $^{\#\#}P < 0.01$ versus the BLM alone-instilled group; $^¶P < 0.05$, $^{¶¶}P < 0.01$ versus BLM+iPSC-MSCs (x1)-treated group.

bands and assessed by densitometry of the relevant bands, which was performed as described above.

2.12. Proteomic profiling of cultured iPSC-MSCs

To further elucidate the immunomodulatory effects of iPSC-MSCs when exposed to inflammatory stimuli *in vitro*, three different iPSC-MSC lines were cultured at a density of 1.5×10^5 cells per well in 6-well plates, in Dulbecco's Modified Eagle Medium with low glucose (DMEM-LG) supplemented with 10 % heat-inactivated FBS (Thermo Fisher Scientific), and allowed to adhere overnight. Subsets of cells within the same plate were left unstimulated or stimulated with recombinant human TNF-α (15 ng/ml; PeproTech via Thermo Fisher Scientific; #300–01 A) and recombinant human IFN-γ (15 ng/ml; PeproTech; #300–02) for 48 hours. After this period, the conditioned media (CM) was collected and filtered using a 0.2 μm filters to remove cell debris. The CM was then processed for LC-MS/MS immediately or aliquots stored at −80°C for further analyses.

Liquid chromatography tandem mass spectrometry (LC-MS/MS) experiments were performed by the Monash Proteomics and Metabolomic Facility (Clayton, VIC, Australia). Proteins were retrieved from 50 μl of CM using 5 μl Strata Clean resin beads per ml of CM (Agilent Technologies, Santa Clara, CA, USA) and further processed for in-gel digestion. 5 μl peptide extract was analysed by LC-MS/MS on an EASY-nLC1000 chromatograph connected to a QExactive HF mass spectrometer (ThermoFisher Scientific) using a Pepmap100 Trap C18 300 mm×5 mm (Thermo Fisher Scientific) and a C18 separation column (3 μm, 100A, 75 μm×15 cm, Nikkyo Technos, Tokyo, Japan) by applying a 120 minute gradient.

LC-MS/MS data was processed with MaxQuant (version 1.5.4.1) using default settings for peak detection, strict trypsin cleavage rule allowing for up to three missed cleavages, variable oxidation on methionine, deamidation of asparagine and glutamine, and acetylation of protein N-termini with strict carbamidomethylation of cysteines. Match between runs was used within each sample group with a retention time window of 1 minute. Label free quantification (LFQ) was performed using classical normalisation with LFQ separated into parameter groups. The fragment spectra were interpreted with the SwissProt Homo sapiens database (version 2016 04) accepting only protein identifications with at least two razor peptides at a 1 % false discovery rate (FDR) cut-off.

For LC-MS/MS data analysis, protein lists retrieved from MaxQuant pipeline were processed using LFQ Analyst [47], removing contaminant proteins, reverse sequences, proteins identified "only by site", and those detected in the unconditioned media control (DMEM-LG + 1:100 ITS). Remaining protein lists were mapped to Gene Ontology term: extracellular space (GO:0005615) (GSEA database https://www.gsea-msigdb.org/gsea/msigdb/human/genesets.jsp?collection=GO:CC) to filter for secreted protein fractions. Where a protein was positively identified in two of three samples within a group the missing value was imputed as the median transformed intensity. Where proteins had at least one positive identification across all samples missing values were imputed from the low end of the Log2 transformed intensity distribution from each individual sample using Perseus (version 1.5.5.3) as suggested by Lazar and colleagues [48].

2.13. Data and statistical analysis

Unless otherwise stated, all data are expressed as the mean ± standard error of the mean (SEM) and were statistically analysed with GraphPad Prism v9.0 (GradPad Software Inc; San Diego, CA, USA) on group sizes of at least n=6, where n refers to the number of independent values from each group described. The *in vivo* data were mainly analysed by a one-way ANOVA and Tukey's post-hoc test to allow for multiple comparisons between groups; whereas non-parametric Kruskal-Wallis tests were used to compare data that was normalised to the saline control group, which was expressed as 1 in each case. The *in vitro* data, which was normalised to the unstimulated cell control group (expressed as 1 in each case), was analysed by a non-parametric Mann-Whitney test. In the case of the HistoIndex analysis of collagen topology, a maximum of n=8 samples per group were analysed; hence, data from n=6–8 samples per group were compared. Differences were considered statistically significant with a *P* value less than 0.05.

3. Results

3.1. Final animal numbers

A double administration of BLM alone, 7-days apart, did not affect the mortality of mice at the dose administered. Hence, n=10 BLM alone injured mice and n=10 saline control mice completed the 5-week protocol. Following iPSC-MSC administration, we found that n=2 mice died after each set of tail vein injections. Hence, for the BLM+iPSC-MSC x1 (single administration) group, n=2 mice died, leaving n=8 mice in that group. For the BLM+iPSC-MSC x2 (double administration) group, n=2 mice died after each set of injections, leaving n=6 mice in that group. It is proposed that this was due to cell aggregation post-tail vein injection in some mice inducing thrombogenesis and/or a pulmonary embolism-induced respiratory failure, rather than the toxic effects of the iPSC-MSCs *per se*. The former are common occurrences, particularly in BLM-injured mice [49–51], which would have exacerbated the breathing capacity of animals that were already inflamed and fibrosed by BLM. The i.v injections were performed by an experienced investigator

3.2. iPSC-MSCs ameliorated lung inflammation, epithelial damage and pro-inflammatory cytokine expression whilst promoting anti-inflammatory cytokine expression in BLM-injured mice

BLM-instilled mice presented with markedly increased lung congestion and inflammatory cell infiltration at day-35 post-injury compared to their saline-instilled counterparts (Fig. 1A). Morphometric analysis of H&E-stained lung sections revealed that interstitial lung inflammation was significantly increased by ~4.3-fold in BLM-instilled mice (mean score of 2.2±0.2), compared to that measured in saline-instilled control mice (mean score of 0.4±0.1; Fig. 1B). Additionally, BLM-instilled mice had significantly increased (by ~1.5-fold; Fig. 1C and D) TSLP-stained epithelial cells at day-35 post-injury, which indicated that these mice had increased lung epithelial damage compared to their saline-instilled controls. In line with the increased inflammation that was detected in BLM-instilled mice, FACS analysis of the BALF demonstrated that various immune cells, including $CD11c^+$ dendritic cells (by ~4.7-fold; Fig. 1E and F), $CD45^+F4/80^+CD206^+$ M2-like

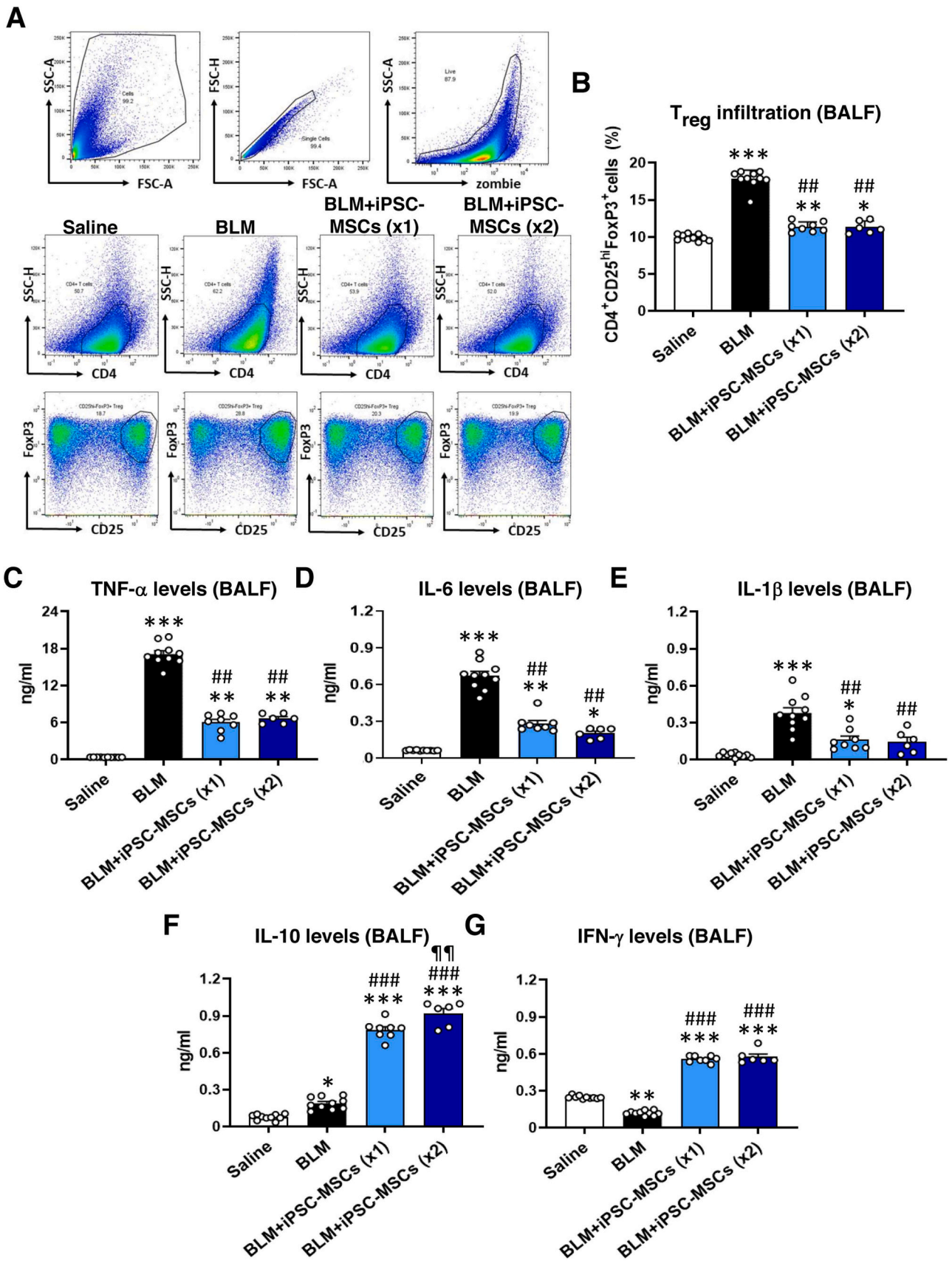

(caption on next page)

Fig. 2. Cynata™-iPSC-MSC-treatment of BLM-injured mice ameliorated T_{reg} infiltration and pro-inflammatory cytokines, whilst promoting anti-inflammatory cytokines levels within the BALF. (A) Representative flow cytometry plots from the BALF samples of each the groups evaluated show the levels of $CD4^+CD25^{hi}FoxP3^+$ cells. The gating strategy used show lavage cells (FSC-A and SSC-A) followed by doublet exclusion based on FSC-A and FSC-H. Live cells were gated based on the Live/Dead exclusion die (zombie-V450) where positive staining indicated dead cells. All gating had been performed on FMO controls and unstained cells. (B-G) Also shown are the mean ± SEM % $CD4^+CD25^{hi}FoxP3^+$ cells (B); pro-inflammatory cytokine levels (ng/ml) including TNF-α (C), IL-6 (D) and IL-1β (E); as well as anti-inflammatory cytokine levels (ng/ml) including IL-10 (F) and IFN-γ (G) within the BALF of each of the groups investigated; from n=6–10 mice per group. $^*P < 0.05$, $^{**}P < 0.01$, $^{***}P < 0.001$ versus the saline-instilled control group; $^{\#\#}P < 0.01$, $^{\#\#\#}P < 0.001$ versus the BLM alone-instilled group; $^{¶¶}P < 0.01$ versus BLM+iPSC-MSCs (x1)-treated group.

macrophages (by ~2.1-fold; Fig. 1G and H) and $CD4^+CD25^{Hi}FoxP3^+$ regulatory T cells (T_{regs}; by ~0.8-fold; Fig. 2A and B) were significantly elevated in these mice, compared to respective measurements obtained from their saline-instilled counterparts. Although a high proportion of $CD4^+$ lymphocytes were detected in the BALF of BLM-injured mice, this was line with previous findings from establishing this model in mice [52]. Furthermore, ELISA analysis of the BALF revealed that pro-inflammatory cytokines such as TNF-α (by ~47-fold; Fig. 2C), IL-6 (by ~9.7-fold; Fig. 2D) and IL-1β (by ~9.3-fold; Fig. 2E), were all significantly increased; whereas anti-inflammatory cytokines such as IL-10 were modestly increased (by ~1.4-fold; Fig. 2F), whilst INF-γ was significantly reduced (by ~0.5-fold; Fig. 2G) in BLM-instilled mice compared to respective measurements from saline-instilled control mice.

For the most part, iPSC-MSC x1 or iPSC-MSC x2 treatment of BLM-injured mice equivalently and significantly reduced the BLM-induced increase in interstitial lung inflammation (by ~35–45 %; Fig. 1A and B), epithelial damage (by ~35–70 %; Fig. 1C and D), immune cell infiltration within the BALF (by ~45–85 %; Fig. 1E-H and Fig. 2A and B) and pro-inflammatory cytokine expression within the BALF (by ~65–75 %; Fig. 2C-E), but markedly elevated pro-inflammatory IL-10 (Fig. 2F) and IFN-γ (Fig. 2G) expression levels within the BALF (by ~4–5-fold). Notably, iPSC-MSC x2 treatment of BLM-injured mice further reduced TSLP-associated epithelial damage (Fig. 1D), dendritic cell infiltration (Fig. 1F) and promoted IL-10 levels (Fig. 2F) to a significantly greater extent than iPSC-MSC x1 treatment.

3.3. iPSC-MSCs ameliorated interstitial lung TGF-β1 expression and canonical TGF-β1 signal transduction in BLM-injured mice

BLM-instilled mice also presented with significantly increased interstitial lung TGF-β1 expression levels (which can be secreted by M2-like macrophages and T_{regs}; by ~8.7-fold) at day-35 post-injury, compared to that measured from saline-instilled control mice (Fig. 3A and B). This was accompanied by a BLM-induced significant increase in canonical lung pSmad2 levels (by ~1.3-fold; Fig. 3C and D), but significantly reduced inhibitory Smad7 levels (by ~0.5-fold; Fig. 3C and F), in the absence of any changes in lung pSmad3 (Fig. 3C and E) or non-canonical pERK1/2 (Fig. 3C and G), pJNK (Fig. 3C and H) or pp38 MAPK (Fig. 3C and I) levels, compared to respective measurements from saline-instilled control animals. iPSC-MSC x1 or iPSC-MSC x2 treatment of BLM-injured mice equivalently and significantly reduced the BLM-induced increase in interstitial lung TGF-β1 expression (by ~78–81 %; Fig. 3A and B), normalised the BLM-induced pSmad2 levels (Fig. 3D) and significantly promoted lung Smad7 levels (by ~2.5-fold and ~4-fold, respectively; Fig. 3F), when administered to BLM-injured mice. These iPSC-MSCs, however, did not affect pSmad3 (Fig. 3E) or non-canonical MAP kinase activity (Fig. 3G-I), highlighting the selective actions of these stem cells.

3.4. iPSC-MSCs abrogated several measures of interstitial lung fibrosis in BLM-injured mice

BLM-instilled mice additionally presented with significantly increased interstitial lung myofibroblast accumulation (by ~14.7-fold; Fig. 4A and B) and Masson's trichrome-stained interstitial extracellular matrix deposition (fibrosis; by ~5.5-fold; Fig. 4C and D) at day-35 post-injury, compared to respective measurements from saline-instilled control mice. This was accompanied by a BLM-induced increase in interstitial lung collagen area to tissue ratio (CART; by ~0.4-fold; Fig. 4E), interstitial collagen fibre density (by ~0.26-fold; Fig. 4F) and interstitial collagen fibre thickness (by ~0.4-fold; Fig. 4G), in the absence of any marked changes in interstitial collagen fibre length (Fig. 4H) or number (Fig. 4I) at the time-point studied, as determined by second harmonic generation analysis of interstitial collagen topology. Whilst iPSC-MSCs x1 or iPSC-MSCs x2 treatment of BLM-instilled mice only partially but significantly reduced the BLM-induced increase in interstitial lung myofibroblast accumulation (by ~38–45 %; Fig. 4B), the once (x1) or once-weekly (x2) i.v-administration of these stem cells equivalently normalised the BLM-induced increase in interstitial lung fibrosis (Fig. 4D), CART (Fig. 4E) and interstitial collagen fibre density (Fig. 4F) and thickness (Fig. 4G), to levels that were no different to that measured in saline-instilled mice. Stem cell treatment also equivalently reduced interstitial collagen fibre length (by ~17–20 %; Fig. 4H), whilst iPSC-MSCs x2 treatment of BLM-instilled mice induced a trend towards an increase in interstitial collagen fibre number (by ~20 %; Fig. 4I).

3.5. iPSC-MSCs promoted the balance between collagen-degrading MMPs and their TIMPs within the lungs of BLM-injured mice

In line with the increased interstitial lung fibrosis that was measured in BLM-instilled mice (Fig. 4), these mice had significantly reduced lung MMP-13 (by ~0.5-fold; Fig. 5A and B), MMP-9 (by ~0.25-fold; Fig. 5A and C) and MMP-2 (by ~0.3-fold; Fig. 5A and D) levels, but a trend towards an increased lung TIMP-1 levels (by ~0.3-fold; Fig. 5A and E) in the absence of any marked changes in lung TIMP-2 levels (Fig. 5A and F) at day-35 post-injury. As a result of this, BLM-instilled mice had significantly reduced MMP-13:TIMP-1 (by ~0.6-fold; Fig. 5G) and MMP-9:TIMP-1 (by ~0.4-fold; Fig. 5H) ratios, and a trends towards a reduced MMP-2:TIMP-2 ratio (by ~0.3-fold; Fig. 5I), compared to respective measurements from saline-instilled control mice.

iPSC-MSC x1 or iPSC-MSC x2 treatment of BLM-injured mice significantly restored the BLM-induced loss of lung MMP-13 (Fig. 5B), MMP-2 (Fig. 5D), MMP-13:TIMP-1 (Fig. 5G), MMP-9:TIMP-1 (Fig. 5H) and MMP-2:TIMP-2 (Fig. 5I) levels to that measured in saline-instilled mice. Notably, whilst iPSC-MSC x1 treatment of BLM-instilled mice restored the BLM-induced loss of lung MMP-13 (Fig. 5B), MMP-13:TIMP-1 (Fig. 5G) and MMP-2:TIMP-2 (Fig. 5I) to corresponding levels measured from saline-instilled mice, iPSC-MSC x2 treatment appeared to further increase lung MMP-13 levels (by ~1.2-fold; Fig. 5B) and the balance between MMP-13 to TIMP-1 (by ~0.9-fold; Fig. 5G) and MMP-2 to TIMP-2 (by ~0.4-fold; Fig. 5I) over that of iPSC-MSC x1 treatment. Furthermore, iPSC-MSC x2 treatment significantly reduced lung TIMP-2 levels compared to that measured in BLM-instilled (by ~0.4-fold) and saline-instilled (by ~0.3-fold; Fig. 5F) mice.

3.6. iPSC-MSCs restored the loss of dynamic lung compliance in BLM-injured mice

In line with the increased interstitial lung inflammation, remodelling and fibrosis that was evident in BLM-instilled mice, these animals underwent a significant loss of dynamic lung compliance in response to the bronchoconstrictor, methacholine (by ~0.4-fold at the highest dose of methacholine tested (50 mg/ml); indicative of these mice having

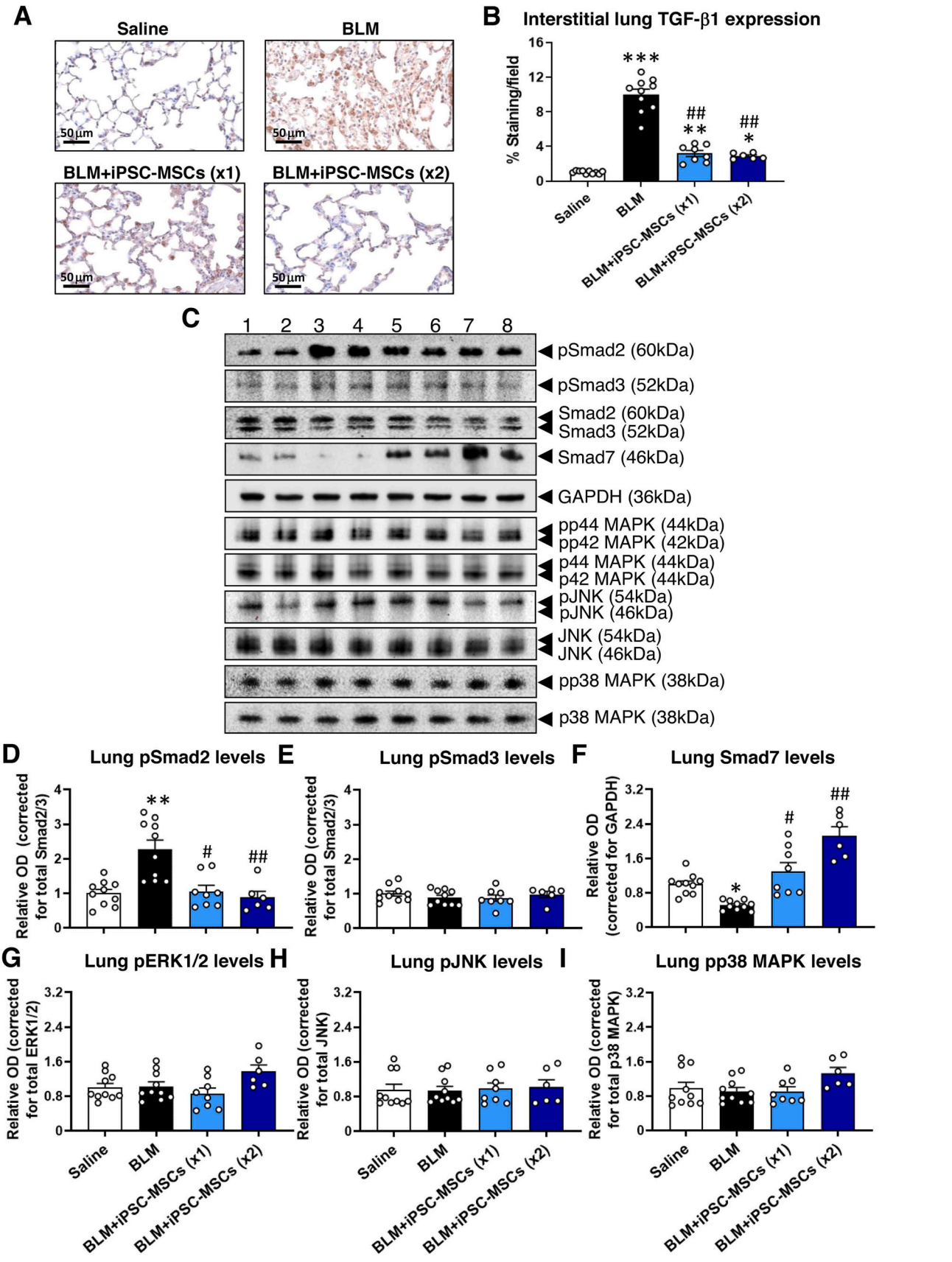

(caption on next page)

Fig. 3. Cynata™-iPSC-MSC-treatment of BLM-injured mice ameliorated lung TGF-β1 expression and canonical TGF-β1 signal transduction. (A) Representative IHC-stained images (at x400 magnification) show the extent of interstitial TGF-β1 expression (brown staining) within the lung of each of the groups investigated. (B) Also shown is the mean ± SEM % interstitial TGF-β1 staining (from 10 non-overlapping fields of view per lung section analysed). (C) Representative Western blots show the extent of canonical TGF-β1 signal transduction in the form of Smad2 phosphorylation (pSmad2), Smad3 phosphorylation (pSmad3) and Smad7; and non-canonical TGF-β1 signal transduction in the form of phosphorylated (p) p44 and p42 mitogen-activated protein kinase (MAPK) (pERK1/2), pJNK and pp38 MAPK in each of the groups investigated. The total Smad2/3, total p44 and p42 MAPK (ERK1/2), total JNK and total p38 MAPK blots were included, respectively, to demonstrate the quality and equivalent loading of protein samples when assessing changes in their phosphorylated forms; whilst a GAPDH blot is included to demonstrate the quality and equivalent loading of Smad7 between the groups analysed. Lanes 1 and 2 are from two separate saline-instilled mice; lanes 3 and 4 are from two separate BLM-instilled mice; lanes 5 and 6 are from two separate BLM+iPSC-MSCs (x1)-treated mice; and lanes 7 and 8 are from two separate BLM+iPSC-MSCs (x2)-treated mice; and the predicted size of each end-point measured is indicated by arrows. The uncropped versions of the blots shown can be found in the Supplementary file; and a further 3-to-4 blots analysing an additional two samples per group demonstrated similar findings. (D-I) Additionally shown are the relative lung mean ± SEM OD of pSmad2 (corrected for total Smad2/3) (D); pSmad3 (corrected for total Smad2/3) (E); Smad7 (corrected for GAPDH) (F); pERK1/2 (corrected for total ERK1/2) (G); pJNK (corrected for total JNK) (H); and pp38 MAPK (corrected for total p38 MAPK) (I); from n=6–10 mice per group. $^{**}P < 0.01$, $^{***}P < 0.001$ versus the saline-instilled control group; $^{\#}P < 0.05$, $^{\#\#}P < 0.01$ versus the BLM alone-instilled group.

stiffened lungs), compared to that measured in saline-instilled control mice (Fig. 6). This BLM-induced loss of dynamic lung compliance was equivalently and significantly restored by iPSC-MSC x1 or iPSC-MSC x2 treatment of BLM-injured mice, to levels measured in saline-instilled healthy control mice.

3.7. Insights into the immunomodulatory effects of iPSC-MSCs

To further assess the immunomodulatory effects of iPSC-MSCs, separately cultured iPSC-MSC lines were stimulated with TNF-α and IFN-γ *in vitro*, which provided an inflammatory stimulus to these stem cells, and are the main cytokines involved in promoting MSC activation and the immunoregulatory effects of MSCs [53]. Following a 48- hour incubation period with these cytokines, iPSC-MSCs were found to significantly promote the protein levels of indoleamine 2,3-dioxygenase 1 (IDO1; by ~68-fold), prostaglandin E synthase 3 (PGTES3; by ~3-fold) and chemokine (C-C motif) ligand 2 (CCL2; by ~4-fold) as part of their ability to markedly down-regulate collagen 1A1 (COL1A1) and collagen 1A2 (COL1A2) protein expression (Fig. 7).

4. Discussion

This study determined for the first time the therapeutic effects of i.v-administered iPSC-MSCs, administered once (x1) or once-weekly over two weeks (x2), in a BLM-induced model of pulmonary fibrosis. Adult C57BL/6 J mice subjected to BLM presented with several key features of human IPF at day-35 post-injury, including interstitial lung inflammation accompanied by immune (dendritic, M2-like macrophage, T_{reg}) cell infiltration and pro-inflammatory cytokine (TNF-α, IL6, IL-1β) expression within the BALF, lung epithelial damage, interstitial lung TGF-β1 expression and canonical signal transduction (increased pSmad2 in conjunction with reduced inhibitory Smad7), interstitial lung myofibroblast accumulation and interstitial lung fibrosis (induced by increased interstitial collagen fibre density and thickness, and collagen to tissue ratio). On the other hand, BLM-injured mice had significantly reduced IFN-γ expression within the BALF, collagenase (MMP-13) and gelatinase (MMP-2, MMP-9) expression levels and MMP to TIMP-1 and TIMP-2 ratios within the lung, and dynamic lung compliance. These findings collectively indicated that these mice had inflamed, fibrosed and stiffened lungs at the time-point studied. It is important to point out that to overcome the resolution of disease pathology that can occur 4–6 weeks after a single administration of BLM to mice [54,55], mice were given two instillations of BLM in this study, 7-days apart. This ensured that a robust therapeutic window was created at the time-point studied, from which the beneficial effects of iPSC-MSCs could be evaluated. Notably, our previous studies had shown that mice subjected to a double administration of BLM, 7-days apart, had established interstitial lung inflammation, fibrosis and a loss of dynamic lung compliance at day-21 post-injury [32], the time-point at which these mice were treated with iPSC-MSCs in the current study.

Strikingly, i.v-administered Cymerus™-generated iPSC-MSCs induced multi-factorial therapeutic effects in BLM-injured mice, whereby a single (x1) or once-weekly (x2) injection of iPSC-MSCs almost equivalently ameliorated several measures of interstitial lung inflammation and epithelial damage, and abrogated several measures of interstitial lung fibrosis to restore the BLM-induced loss of dynamic lung compliance. Not only did these iPSC-MSCs ablate the impact of lung inflammation, epithelial damage, TGF-β1 and myofibroblast activity on newly-formed ECM/collagen deposition, they clearly increased the balance between various collagen-degrading MMPs and their TIMPs, which would allow for the MMP-induced breakdown of established collagen-induced fibrosis. These collective actions likely explained how these iPSC-MSCs rapidly normalised several measures of lung fibrosis including interstitial lung collagen area to tissue ratio, and collagen fibre density, thickness and length.

In line with the immunosuppressive effects of iPSC-MSCs that have been shown in other disease settings [56,57], these Cynata™-iPSC-MSCs ameliorated BLM-induced inflammation at the level of dendritic cell, M2-like macrophage and Treg infiltration, and via the inhibition of pro-inflammatory cytokines such as TNF-α, IL-6 and IL-1β, whilst promoting the actions of anti-inflammatory cytokines such as IL-10 and IFN-γ. Dendritic cells are involved in initiating various T cell functions [58], are a source of TNF-α [59] and IL-6 [60], and can mediate adaptive immune system-induced organ inflammation. On the other hand, M2-like macrophages are a major source of TNF-α, IL-6, IL-1β, IL-10 and TGF-β1 [61], and play a key role in promoting wound-healing. However, persistent M2-like macrophage accumulation and activation can contribute to aberrant TGF-β1-induced fibrosis progression. Tregs can adopt differential roles in pulmonary fibrosis, but when allowed to accumulate, can also secrete and promote the TGF-β1-induced progression of interstitial collagen-associated fibrosis [62]. Hence, the iPSC-MSC-induced amelioration of this immune cell infiltration likely mitigated various pro-inflammatory and pro-fibrotic factors that were secreted by these cells, that contributed to interstitial fibrosis progression when persistently activated.

When cultured *in vitro* and stimulated with TNF-α and IFN-γ, further insights into the immunomodulatory effects of these iPSC-MSCs were observed, particularly with the ability of these stimulated cells to promote IDO1, PTGES3 and CCL2 protein levels as part of their anti-fibrotic effects on COL1A1 and COL1A2 protein expression. IDO1 is a key rate-limiting enzyme that is produced by DCs, that converts tryptophan to kynurenine and inhibits immune cell effector function and/or facilitates the death of T cells [63]. MSCs do not innately express IDO1, but have been found to up-regulate IDO1 in the presence of inflammatory (TNF-α, IFN-γ and/or IL-1β) stimuli [64]. PTGES3 is also an enzyme that converts prostaglandin endoperoxide H2 to prostaglandin E2 (PGE2), and can induce immunosuppressive effects in the lung [65]. Although it has mainly been studied in the context of cancer, the down-regulation of PTGES3 has been found to correlate with enhanced lung inflammation in infants and children with cystic fibrosis, that have been exposed to second hand cigarette smoke [66]. Additionally, as immune cells recruited by CCL2 (also known as monocyte chemoattractant protein 1)

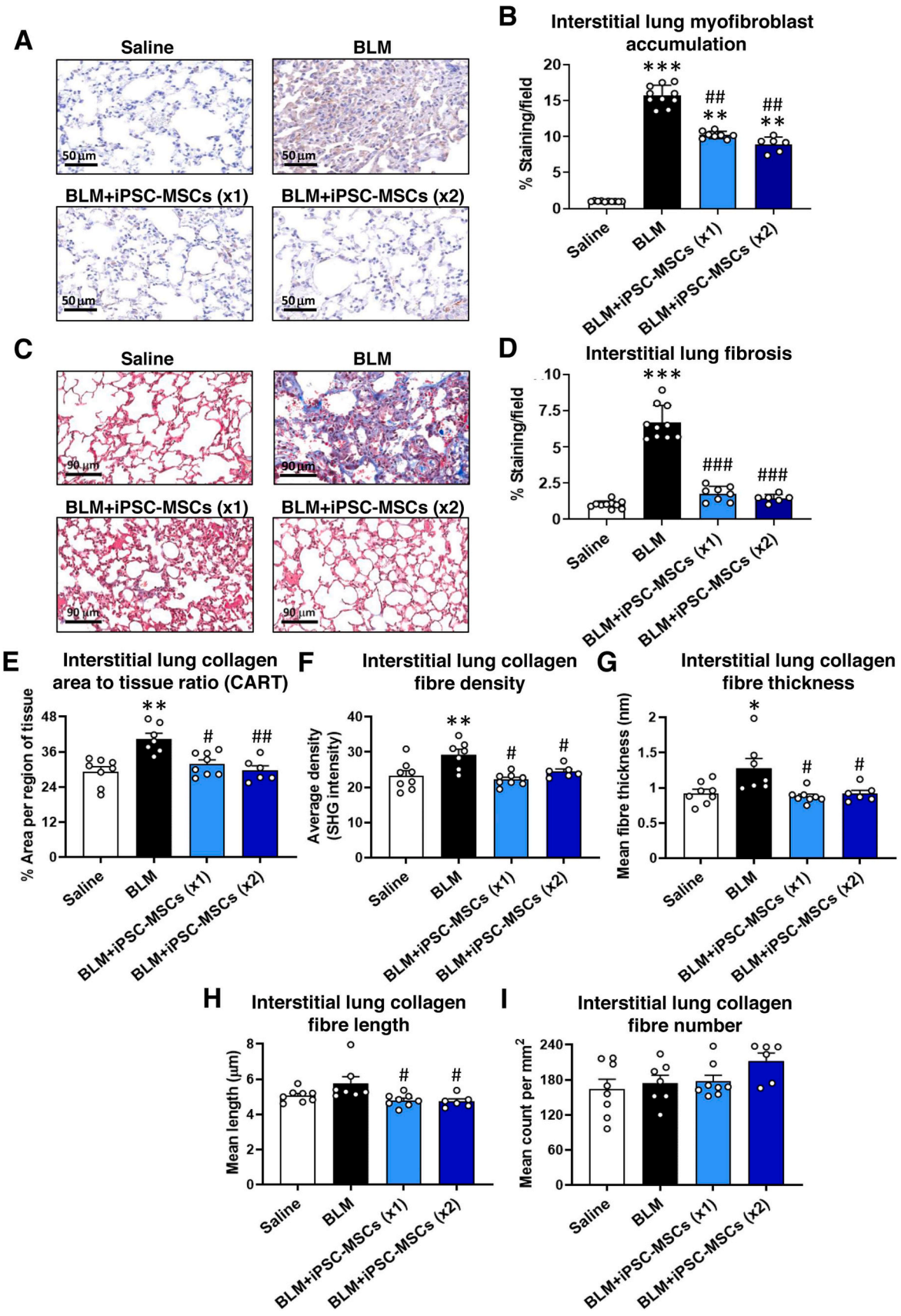

(caption on next page)

Fig. 4. Cynata™-iPSC-MSC-treatment of BLM-injured mice abrogated several measures of BLM-induced lung fibrosis. (A,C) Representative α-SMA- (A) and Masson's trichrome- (C) stained images (at x400 magnification) show the extent of interstitial myofibroblast accumulation (brown staining) (A) and ECM deposition (blue staining) (C) within the lung of each of the groups investigated. Scale bar = 50 μm (A) or 90 μm (C). (B,D) Also shown are the mean ± SEM % interstitial myofibroblast accumulation within the lung (from 10 non-overlapping fields of view per lung section analysed) (B) and interstitial lung fibrosis (ECM deposition; from 10 non-overlapping fields of view per lung section analysed) (D) from n=6–10 mice per group. (E-I) Additionally shown are the mean ± SEM interstitial lung collagen area to tissue ratio (CART) (E); interstitial lung collagen fibre density (F); interstitial lung collagen fibre thickness (G); interstitial lung collagen fibre length (H); and interstitial lung collagen fibre number (I) from n=6–8 mice per group. $^{*}P < 0.05$, $^{**}P < 0.01$, $^{***}P < 0.001$ versus the saline-instilled control group; $^{\#}P < 0.05$, $^{\#\#}P < 0.01$, $^{\#\#\#}P < 0.001$ versus the BLM alone-instilled group.

play immunosuppressive roles, the iPSC-MSC-induced activation of CCL2 (along with IDO1 and PTGES3) may have contributed to the immune cell-dampening and anti-inflammatory effects of these stem cells. Notably, as CCL2 release and chemotaxis by monocytes is promoted by IL-10 [67], it could be suggested that therapeutic effects of iPSC-MSCs were partly mediated via their ability to up-regulate the IL-10-CCL2 axis [68].

Cynata™-iPSC-MSCs also markedly reduced lung epithelial damage, in line with the angiogenic and wound-healing properties of these cells. Previous studies had found that an intra-myocardial injection of (5×10^6) Cynata™-iPSC-MSCs to rats with myocardial infarction, promoted arteriogenesis and the branching and sprouting of microvessels with the heart [69], which could also be induced in the lung. Cynata™-iPSC-MSCs were also found to express IL-8, TIMP-1 and TIMP-2, regulated upon activation, normal T cell expressed and presumably secreted (RANTES) and vascular endothelial growth factor (VEGF) [60], which are all involved in neovascularization. Furthermore, iPSC-MSCs promoted epithelial cell proliferation via a tumor necrosis factor-α-stimulated gene 6 (TSG-6)- and Akt-dependent manner [70]. TSG-6 in turn, attenuated bleomycin-induced lung inflammatory cell infiltration, fibrosis, and the deterioration of lung function in mice [71]. Consistent with these findings, it has been proposed that the extracellular vesicles secreted by iPSC-MSCs, that contain the therapeutic and reparative components of these cells, have an enhanced ability to regulate the microenvironment and promote tissue repair, compared to tissue-derived MSCs [72].

Whilst the viability and efficacy of other implanted stem cells can be impaired by the build-up and presence of fibrosis [73,74], remarkably these iPSC-MSCs abrogated the established interstitial fibrosis that had developed in BLM-injured mice following a single or once-weekly administration. Likewise, the once-weekly i.v- or intranasal application of iPSC-MSCs (over a 2-week period) markedly reduced the established airway fibrosis that had developed in mice subjected to 9-weeks of chronic AAD [26]. Although these iPSC-MSCs only partially impaired the BLM-induced increase in myofibroblast differentiation and accumulation (and hence, myofibroblast-mediated ECM production), this was likely mediated by their amelioration of pro-fibrotic TGF-β1 activity (via the inhibition of pSmad2 and promotion of Smad7) on fibroblast to myofibroblast differentiation. It is also possible that these iPSC-MSCs may have promoted the de-differentiation of a portion of myofibroblasts back to fibroblast-like cells, through their inhibition of the TGF-β1/pSmad2 axis [75]; although further studies are required to validate this. The additional ability of these cells to promote the balance between various collagen-degrading MMPs and their natural (TIMP) inhibitors, also likely allowed for these cells to stimulate the MMP-induced breakdown of existing BLM-induced collagen deposition. This resulted in iPSC-MSC-treated BLM-injured mice having a markedly reduced interstitial lung collagen to tissue ratio (CART) and characteristics of degraded interstitial lung collagen fibres, compared to their untreated counterparts. Based on these findings, it could be further suggested that iPSC-MSCs may provide a better therapeutic alternative to pirfenidone or nintedanib as a treatment for IPF, as these currently-used drugs only suppress pro-fibrotic cytokine and related receptor activity on myofibroblast-induced fibrogenesis [10–14], but do not resolve established fibrotic disease pathology.

Notably, a once-weekly administration of iPSC-MSCs only reduced TSLP-associated lung epithelial damage and promoted anti-inflammatory IL-10 levels to a greater extent than a single administration of cells, but did not further impact on measures of fibrosis or dynamic lung compliance in BLM-injured mice. These findings conferred that interstitial fibrosis is the key contributor to lung function decline in IPF, and that the targeting of other features of disease pathology, such as epithelial damage or inflammation, are unlikely to have a major impact on alleviating the lung dysfunction associated with established disease. To this extent, it was demonstrated that a single injection of iPSC-MSCs maintained therapeutic efficacy after two weeks of administration and restored the BLM-induced loss of dynamic lung compliance back to that measured in healthy control mice. However, whether the therapeutic effects of these cells are maintained for longer periods of time, or require fortnightly or monthly dosing to maintain their effects requires further investigation. Again though, this is potentially another advantage that these iPSC-MSCs provide as a therapeutic option for IPF over pirfenidone or nintedanib, as these currently-used medications require daily and multiple administrations per day to maintain their preventative effects.

5. Conclusion

The findings of this study have demonstrated the therapeutic value of Cynata iPSC-MSCs as a novel treatment option for IPF, albeit from studies conducted in mice. These stem cells not only inhibited TGF-β1 signal transduction and myofibroblast-induced fibrogenesis, they promoted the balance between collagen-degrading MMPs and their natural inhibitors, which appeared to allow for the MMP-induced breakdown of interstitial collagen fibres; effects that were maintained over a fortnight following a single administration of iPSC-MSCs. Whilst the safety of these cells has already been demonstrated in a clinical setting [76], further studies evaluating the dosing and timing of these iPSC-MSCs in primates or larger preclinical models, and the comparison of these iPSC-MSCs with currently-used medications such as pirfenidone and nintedanib, will be key to developing the therapeutic potential of these stem cells as a viable treatment for IPF.

CRediT authorship contribution statement

Amlan Chakraborty: Writing – review & editing, Methodology, Investigation, Formal analysis. **Chao Wang:** Writing – review & editing, Methodology, Investigation, Formal analysis. **Margeaux Hodgson-Garms:** Formal analysis, Investigation, Methodology, Writing – review & editing. **Brad R.S. Broughton:** Writing – review & editing, Methodology, Investigation. **Jessica E. Frith:** Formal analysis, Supervision, Writing – review & editing. **Kilian Kelly:** Writing – review & editing, Resources, Conceptualization. **Chrishan S. Samuel:** Writing – original draft, Supervision, Project administration, Investigation, Funding acquisition, Formal analysis, Data curation, Conceptualization.

Funding

This work was supported by funding from Cynata Therapeutics Ltd to C. S. Samuel and J. E. Frith; and a Monash Biomedicine Discovery Institute (BDI) Discovery Fellowship to C. S. Samuel.

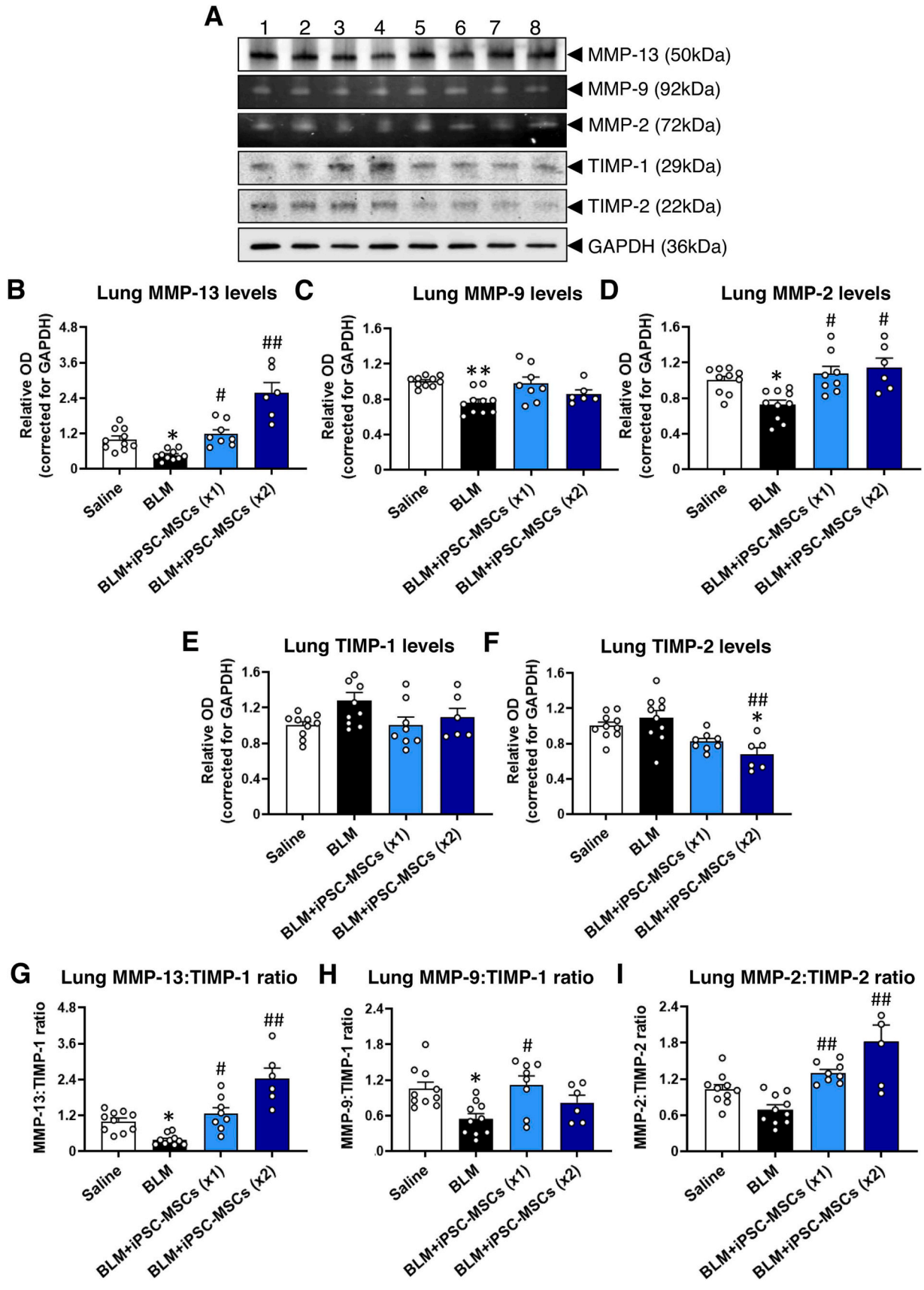

(caption on next page)

Fig. 5. Cynata™-iPSC-MSC-treatment of BLM-injured mice increased the balance between lung collagen-degrading MMPs and their natural inhibitors (TIMPs). (A) Representative Western blots or zymographs show the extent of MMP-13 (collagenase-3), MMP-9 (gelatinase B), MMP-2 (gelainase A), TIMP-1 and TIMP-1 in each of the groups investigated. A GAPDH blot is also included to demonstrate the quality and equivalent loading of the protein samples loaded. Lanes 1 and 2 are from two separate saline-instilled mice; lanes 3 and 4 are from two separate BLM-instilled mice; lanes 5 and 6 are from two separate BLM+iPSC-MSCs (x1)-treated mice; and lanes 7 and 8 are from two separate BLM+iPSC-MSCs (x2)-treated mice; and the predicted size of each end-point measured is indicated by arrows. The uncropped versions of the blots shown can be found in the Supplementary file; and a further 3-to-4 blots analysing an additional two samples per group demonstrated similar findings. (B-F) Also shown are the relative mean ± SEM OD lung MMP-13 (B); lung MMP-9 (C); lung MMP-2 (D); lung TIMP-1 (E); and lung TIMP-2 (F) levels (all corrected for corresponding GAPDH expression) from n=6–10 mice per group. (G-I) Additionally shown are the lung MMP-13:TIMP-1 ratio (G), lung MMP-9:TIMP-1 ratio (H); and lung MMP-2:TIMP-2 ratio (I) from n=6–10 mice per group. $^{*}P < 0.05$, $^{**}P < 0.01$ versus the saline-instilled control group; $^{\#}P < 0.05$, $^{\#\#}P < 0.01$ versus the BLM alone-instilled group.

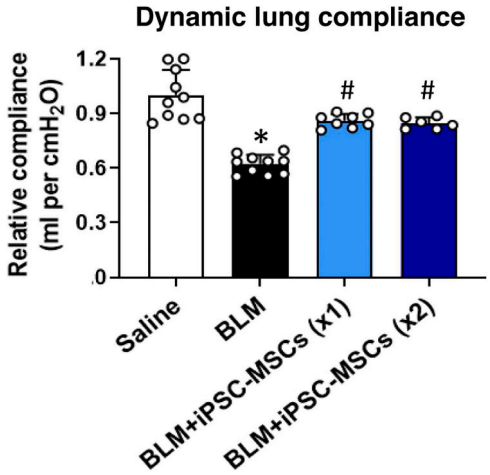

Fig. 6. Cynata™-iPSC-MSC-treatment of BLM-injured mice restored the BLM-induced loss of dynamic lung compliance (stiffness). Shown is the relative lung compliance (measured as ml per cmH_2O) in each of the groups evaluated, in response to the highest dose of methacholine (bronchoconstrictor) administered (50 mg/ml); from n=6–10 mice per group. $^{*}P < 0.05$ versus the saline-instilled control group; $^{\#}P < 0.05$ versus the BLM alone-instilled group.

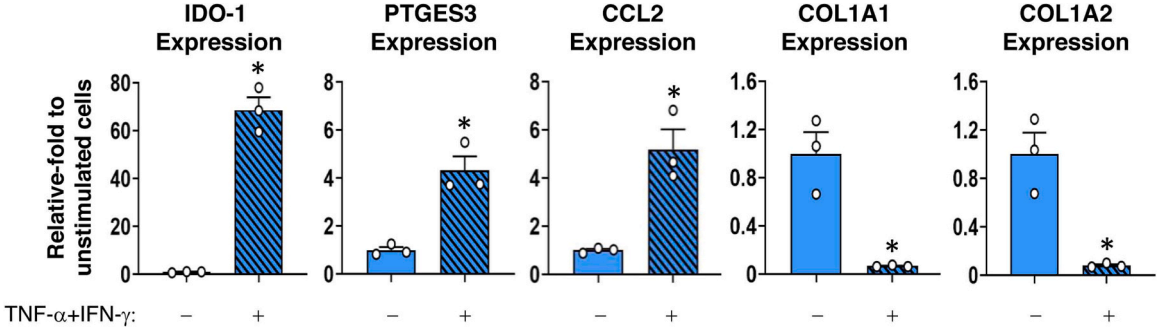

Fig. 7. The immunomodulatory effects of cultured Cynata™-iPSC-MSCs that contributed to their anti-fibrotic effects on collagen 1 protein expression. Shown is the relative mean ± SEM protein expression levels of IDO1, PTGES3, CCL2, COL1A1 and COL1A2, from n=3 separate Cynata™-iPSC-MSCs lines, that were left unstimulated or were stimulated with TNF-α and IFN-γ for 48- hours; as determined by LC-MS/MS analysis of the conditioned media. $^{*}P < 0.05$ versus the respective levels of each protein analysed from the unstimulated cell group.

Declaration of Competing Interest

All Authors have nothing to disclose.

Data availability

Data will be made available on request.

References

[1] S.G. Royce, Y. Moodley, C.S. Samuel, Novel therapeutic strategies for lung disorders associated with airway remodelling and fibrosis, Pharmacol. Ther. 141 (2014) 250–260.

[2] B. Selvarajah, M. Plate, R.C. Chambers, Pulmonary fibrosis: emerging diagnostic and therapeutic strategies, Mol. Asp. Med. 94 (2023) 101227.

[3] P. Spagnolo, J.S. Lee, Recent advances in the genetics of idiopathic pulmonary fibrosis, Curr. Opin. Pulm. Med. 29 (2023) 399–405.

[4] S.A. Gandhi, B. Min, J.C. Fazio, K.A. Johannson, C. Steinmaus, C.J. Reynolds, K. J. Cummings, The impact of occupational exposures on the risk of idiopathic pulmonary fibrosis: a systematic review and meta-analysis, Ann. Am. Thorac. Soc. 21 (2024) 486–498.

[5] L. Nalysnyk, J. Cid-Ruzafa, P. Rotella, D. Esser, Incidence and prevalence of idiopathic pulmonary fibrosis: review of the literature, Eur. Respir. Rev. 21 (2012) 355–361.

[6] I.A. Cox, P. Otahal, B. de Graaff, T.J. Corte, Y. Moodley, C. Zappala, I. Glaspole, P. Hopkins, S. Macansh, E.H. Walters, A.J. Palmer, Incidence, prevalence and mortality of idiopathic pulmonary fibrosis in Australia, Respirology 27 (2022) 209–216.

[7] A.J. Podolanczuk, C.C. Thomson, M. Remy-Jardin, L. Richeldi, F.J. Martinez, M. Kolb, G. Raghu, Idiopathic pulmonary fibrosis: state of the art for 2023, Eur. Respir. J. 61 (2023) 2200957.
[8] D. Bouros, K.M. Antoniou, Current and future therapeutic approaches in idiopathic pulmonary fibrosis, Eur. Respir. J. 26 (2005) 693–702.
[9] J.C. Horowitz, V.J. Thannickal, Idiopathic pulmonary fibrosis: new concepts in pathogenesis and implications for drug therapy, Treat. Respir. Med. 5 (2006) 325–342.
[10] T.E. King, W.Z. Bradford, S. Castro-Bernardini, E.A. Fagan, I. Glaspole, M. K. Glassberg, E. Gorina, P.M. Hopkins, D. Kardatzke, L. Lancaster, D.J. Lederer, S. D. Nathan, C.A. Pereira, S.A. Sahn, R. Sussman, J.J. Swigris, P.W. Noble, A phase 3 trial of pirfenidone in patients with idiopathic pulmonary fibrosis, N. Eng. J. Med. 370 (2014) 2083–2092.
[11] P.W. Noble, C. Albera, W.Z. Bradford, U. Costabel, M.K. Glassberg, D. Kardatzke, T. E. King Jr., L. Lancaster, S.A. Sahn, J. Szwarcberg, D. Valeyre, R.M. du Bois, C. S. Group, Pirfenidone in patients with idiopathic pulmonary fibrosis (CAPACITY): two randomised trials, Lancet 377 (2011) 1760–1769.
[12] Y. Taguchi, M. Ebina, S. Hashimoto, T. Ogura, A. Azuma, H. Taniguchi, Y. Kondoh, M. Suga, H. Takahashi, K. Nakata, Y. Sugiyama, S. Kudoh, T. Nukiwa, J. Pirfenidone Clinical Study Group in, Efficacy of pirfenidone and disease severity of idiopathic pulmonary fibrosis: extended analysis of phase III trial in Japan, Respir, Investig 53 (2015) 279–287.
[13] K.R. Flaherty, C.D. Fell, J.T. Huggins, H. Nunes, R. Sussman, C. Valenzuela, U. Petzinger, J.L. Stauffer, F. Gilberg, M. Bengus, M. Wijsenbeek, Safety of nintedanib added to pirfenidone treatment for idiopathic pulmonary fibrosis, Eur. Respir. J. 52 (2018) 1800230.
[14] S. Davis, R. Rafia, C. Carroll, J. Hamilton, M. Essat, Pirfenidone for treating idiopathic pulmonary fibrosis: an evidence review group perspective of a NICE single technology appraisal, Pharmacoeconomics 37 (2019) 763–775.
[15] H. Taniguchi, M. Ebina, Y. Kondoh, T. Ogura, A. Azuma, M. Suga, Y. Taguchi, H. Takahashi, K. Nakata, A. Sato, M. Takeuchi, G. Raghu, S. Kudoh, T. Nukiwa, J. Pirfenidone in idiopathic pulmonary fibrosis, Eur. Respir. J. 35 (2010) 821–829.
[16] M. Zurkova, E. Kriegova, V. Kolek, V. Lostakova, M. Sterclova, V. Bartos, M. Doubkova, I. Binkova, M. Svoboda, J. Strenkova, M. Janotova, M. Plackova, L. Lacina, V. Rihak, F. Petrik, P. Lisa, R. Bittenglova, R. Tyl, G. Ondrejka, H. Suldova, J. Lnenicka, J. Psikalova, T. Snizek, J. Homolka, R. Kralova, J. Kervitzer, M. Vasakova, I.L.D. section, I.P.F. registry, Effect of pirfenidone on lung function decline and survival: 5-yr experience from a real-life IPF cohort from the Czech EMPIRE registry, Respir. Res. 20 (2019) 16.
[17] K. English, B.P. Mahon, K.J. Wood, Mesenchymal stromal cells; role in tissue repair, drug discovery and immune modulation, Curr. Drug Deliv. 11 (2014) 561–571.
[18] V. Sueblinvong, D.J. Weiss, Stem cells and cell therapy approaches in lung biology and diseases, Transl. Res. 156 (2010) 188–205.
[19] S.A. Jacobs, V.D. Roobrouck, C.M. Verfaillie, S.W. Van Gool, Immunological characteristics of human mesenchymal stem cells and multipotent adult progenitor cells, Immunol. Cell Biol. 91 (2013) 32–39.
[20] A.C. Inamdar, A.A. Inamdar, Mesenchymal stem cell therapy in lung disorders: pathogenesis of lung diseases and mechanism of action of mesenchymal stem cell, Exp. Lung Res. 39 (2013) 315–327.
[21] R. Lim, P. Milton, S.V. Murphy, H. Dickinson, S.T. Chan, G. Jenkin, Human mesenchymal stem cells reduce lung injury in immunocompromised mice but not in immunocompetent mice, Respiration 85 (2013) 332–341.
[22] P. Mancheno-Corvo, R. Menta, B. del Rio, M. Franquesa, C. Ramirez, M. J. Hoogduijn, O. DelaRosa, W. Dalemans, E. Lombardo, T Lymphocyte prestimulation impairs in a time-dependent manner the capacity of adipose mesenchymal stem cells to inhibit proliferation: role of interferon gamma, poly I:C, and tryptophan metabolism in restoring adipose mesenchymal stem cell inhibitory effect, Stem Cells Dev. 24 (2015) 2158–2170.
[23] D.J. Weiss, Concise review: current status of stem cells and regenerative medicine in lung biology and diseases, Stem Cells 32 (2014) 16–25.
[24] M.A. Vodyanik, J. Yu, X. Zhang, S. Tian, R. Stewart, J.A. Thomson, I.I. Slukvin, A mesoderm-derived precursor for mesenchymal stem and endothelial cells, Cell Stem Cell 7 (2010) 718–729.
[25] S.G. Royce, W. Mao, R. Lim, K. Kelly, C.S. Samuel, iPSC- and mesenchymoangioblast-derived mesenchymal stem cells provide greater protection against experimental chronic allergic airways disease compared with a clinically used corticosteroid, FASEB J. 33 (2019) 6402–6411.
[26] S.G. Royce, S. Rele, B.R.S. Broughton, K. Kelly, C.S. Samuel, Intranasal administration of mesenchymoangioblast-derived mesenchymal stem cells abrogates airway fibrosis and airway hyperresponsiveness associated with chronic allergic airways disease, FASEB J. 31 (2017) 4168–4178.
[27] J.D. Williamson, L.R. Sadofsky, S.P. Hart, The pathogenesis of bleomycin-induced lung injury in animals and its applicability to human idiopathic pulmonary fibrosis, Exp. Lung Res. 41 (2015) 57–73.
[28] R. Lamichhane, S. Patial, Y. Saini, Higher susceptibility of males to bleomycin-induced pulmonary inflammation is associated with sex-specific transcriptomic differences in myeloid cells, Toxicol. Appl. Pharmacol. 454 (2022) 116228.
[29] E.F. Redente, K.M. Jacobsen, J.J. Solomon, A.R. Lara, S. Faubel, R.C. Keith, P. M. Henson, G.P. Downey, D.W. Riches, Age and sex dimorphisms contribute to the severity of bleomycin-induced lung injury and fibrosis, Am. J. Physiol. Lung Cell. Mol. Physiol. 301 (2011) L510–L518.
[30] Y. Moodley, S. Ilancheran, C. Samuel, V. Vaghjiani, D. Atienza, E.D. Williams, G. Jenkin, E. Wallace, A. Trounson, U. Manuelpillai, Human amnion epithelial cell transplantation abrogates lung fibrosis and augments repair, Am. J. Respir. Crit. Care Med. 182 (2010) 643–651.
[31] R.H. Lee, A.A. Pulin, M.J. Seo, D.J. Kota, J. Ylostalo, B.L. Larson, L. Semprun-Prieto, P. Delafontaine, D.J. Prockop, Intravenous hMSCs improve myocardial infarction in mice because cells embolized in lung are activated to secrete the anti-inflammatory protein TSG-6, Cell Stem Cell 5 (2009) 54–63.
[32] S.G. Royce, K.P. Patel, W. Mao, D. Zhu, R. Lim, C.S. Samuel, Serelaxin enhances the therapeutic effects of human amnion epithelial cell-derived exosomes in experimental models of lung disease, Br. J. Pharmacol. 176 (2019) 2195–2208.
[33] K.P. Patel, A.S. Giraud, C.S. Samuel, S.G. Royce, Combining an epithelial repair factor and anti-fibrotic with a corticosteroid offers optimal treatment for allergic airways disease, Br. J. Pharmacol. 173 (2016) 2016–2029.
[34] W. Mitzner, S. Blosser, D. Yager, E. Wagner, Effect of bronchial smooth muscle contraction on lung compliance, J. Appl. Physiol. 72 (1992) 158–167.
[35] N.R. Locke, S.G. Royce, J.S. Wainewright, C.S. Samuel, M.L. Tang, Comparison of airway remodeling in acute, subacute, and chronic models of allergic airways disease, Am. J. Respir. Cell Mol. Biol. 36 (2007) 625–632.
[36] G.J. Randolph, C. Jakubzick, C. Qu, Antigen presentation by monocytes and monocyte-derived cells, Curr. Opin. Immunol. 20 (2008) 52–60.
[37] W. Lancelin, A. Guerrero-Plata, Isolation of mouse lung dendritic cells, J. Vis. Exp. (57) (2011) 3563.
[38] A.N. Desch, P.M. Henson, C.V. Jakubzick, Pulmonary dendritic cell development and antigen acquisition, Immunol. Res. 55 (2013) 178–186.
[39] R. Herro, R. Da Silva Antunes, A.R. Aguilera, K. Tamada, M. Croft, Tumor necrosis factor superfamily 14 (LIGHT) controls thymic stromal lymphopoietin to drive pulmonary fibrosis, J. Allergy Clin. Immunol. 136 (2015) 757–768.
[40] X. Xu, H. Dai, J. Zhang, The potential role of interleukin (IL)-25/IL-33/thymic stromal lymphopoietin (TSLP) on the pathogenesis of idiopathic pulmonary fibrosis, Clin. Respir. J. 16 (2022) 696–707.
[41] S. Bhuiyan, M. Shen, S. Chelvaretnam, A.Y. Tan, G. Ho, M.A. Hossain, R.E. Widdop, C.S. Samuel, Assessment of renal fibrosis and anti-fibrotic agents using a novel diagnostic and stain-free second-harmonic generation platform, FASEB J. 35 (2021) e21595.
[42] F.T. Caceres, T.A. Gaspari, C.S. Samuel, A.A. Pinar, Serelaxin inhibits the profibrotic TGF-beta1/IL-1beta axis by targeting TLR-4 and the NLRP3 inflammasome in cardiac myofibroblasts, FASEB J. 33 (2019) 14717–14733.
[43] C. Wang, T.A. Gaspari, D. Ferens, I. Spizzo, B.K. Kemp-Harper, C.S. Samuel, Simultaneous targeting of oxidative stress and fibrosis reverses cardiomyopathy-induced ventricular remodelling and dysfunction, Br. J. Pharmacol. 178 (2021) 2424–2442.
[44] N. Khalil, O. Bereznay, M. Sporn, A.H. Greenberg, Macrophage production of transforming growth factor beta and fibroblast collagen synthesis in chronic pulmonary inflammation, J. Exp. Med. 170 (1989) 727–737.
[45] S.H. Phan, S.L. Kunkel, Lung cytokine production in bleomycin-induced pulmonary fibrosis, Exp. Lung Res. 18 (1992) 29–43.
[46] J.F. Woessner Jr., Quantification of matrix metalloproteinases in tissue samples, Methods Enzym. 248 (1995) 510–528.
[47] A.D. Shah, R.J.A. Goode, C. Huang, D.R. Powell, R.B. Schittenhelm, Lfq-Analyst: an easy-To-use interactive web platform to analyze and visualize label-free proteomics data preprocessed with maxquant, J. Proteome Res. 19 (2019) 204–211.
[48] C. Lazar, L. Gatto, M. Ferro, C. Bruley, T. Burger, Accounting for the multiple natures of missing values in label-free quantitative proteomics data sets to compare imputation strategies, J. Proteome Res. 15 (2016) 1116–1125.
[49] D. Furlani, M. Ugurlucan, L. Ong, K. Bieback, E. Pittermann, I. Westien, W. Wang, C. Yerebakan, W. Li, R. Gaebel, R.K. Li, B. Vollmar, G. Steinhoff, N. Ma, Is the intravascular administration of mesenchymal stem cells safe? Mesenchymal stem cells and intravital microscopy, Microvasc. Res. 77 (2009) 370–376.
[50] Y. Takahashi, O. Tsuji, G. Kumagai, C.M. Hara, H.J. Okano, A. Miyawaki, Y. Toyama, H. Okano, M. Nakamura, Comparative study of methods for administering neural stem/progenitor cells to treat spinal cord injury in mice, Cell Transpl. 20 (2011) 727–739.
[51] L. Coppin, E. Sokal, X. Stephenne, Thrombogenic risk induced by intravascular mesenchymal stem cell therapy: current status and future perspectives, Cells 8 (2019) 1160.
[52] G. Izbicki, M.J. Segel, T.G. Christensen, M.W. Conner, R. Breuer, Time course of bleomycin-induced lung fibrosis, Int. J. Exp. Pathol. 83 (2002) 111–119.
[53] L. Lopez-Garcia, M.E. Castro-Manrreza, TNF-α and IFN-γ participate in improving the immunoregulatory capacity of mesenchymal stem/stromal cells: importance of cell-cell contact and extracellular vesicles, Int. J. Mol. Sci. 22 (2021) 9531.
[54] M.P. Chung, M.M. Monick, N.Y. Hamzeh, N.S. Butler, L.S. Powers, G. W. Hunninghake, Role of repeated lung injury and genetic background in bleomycin-induced fibrosis, Am. J. Respir. Cell Mol. Biol. 29 (2003) 375–380.
[55] P. Kolb, C. Upagupta, M. Vierhout, E. Ayaub, P.S. Bellaye, J. Gauldie, C. Shimbori, M. Inman, K. Ask, M.R.J. Kolb, The importance of interventional timing in the bleomycin model of pulmonary fibrosis, Eur. Respir. J. 55 (2020) 1901105.
[56] E.I. Ozay, J. Vijayaraghavan, G. Gonzalez-Perez, S. Shanthalingam, H.L. Sherman, D.T. Garrigan Jr., K. Chandiran, J.A. Torres, B.A. Osborne, G.N. Tew, Slukvin II, R. A. Macdonald, K. Kelly, L.M. Minter, Cymerus iPSC-MSCs significantly prolong survival in a pre-clinical, humanized mouse model of Graft-vs-host disease, Stem Cell Res. 35 (2019) 101401.
[57] S.E. Spellicy, D.C. Hess, The immunomodulatory capacity of induced pluripotent stem cells in the post-stroke environment, Front. Cell Dev. Biol. 9 (2021) 647415.
[58] F. Sallusto, A. Lanzavecchia, The instructive role of dendritic cells on T-cell responses, Arthritis Res. 4 (Suppl 3) (2002) S127–S132.
[59] P. Blanco, A.K. Palucka, V. Pascual, J. Banchereau, Dendritic cells and cytokines in human inflammatory and autoimmune diseases, Cytokine Growth Factor Rev. 19 (2008) 41–52.

[60] Y.D. Xu, M. Cheng, P.P. Shang, Y.Q. Yang, Role of IL-6 in dendritic cell functions, J. Leukoc. Biol. 111 (2022) 695–709.
[61] T. Roszer, Understanding the mysterious M2 macrophage through activation markers and effector mechanisms, Mediat. Inflamm. 2015 (2015) 816460.
[62] S.Z. Birjandi, V. Palchevskiy, Y.Y. Xue, S. Nunez, R. Kern, S.S. Weigt, J.P. Lynch, 3rd, T.A. Chatila, J.A. Belperio, CD4(+)CD25(hi)Foxp3(+) cells exacerbate bleomycin-induced pulmonary fibrosis, Am. J. Pathol. 186 (2016) 2008–2020.
[63] J.C. Mbongue, D.A. Nicholas, T.W. Torrez, N.S. Kim, A.,F. Firek, W.H.R. Langridge, The role of indoleamine 2, 3-dioxygenase in immune supression and autoimmunity, Vaccines 3 (2015) 703–729.
[64] J. Su, X. Chen, Y. Huang, W. Li, J. Li, K. Cao, G. Cao, L. Zhang, F. Li, A.I. Roberts, H. Kang, P. Yu, G. Ren, W. Ji, Y. Wang, Y. Shi, Phylogenetic distinction of iNOS and IDO function in mesenchymal stem cell-mediated immunosuppression in mammalian species, Cell Death Differ. 21 (2014) 388–396.
[65] T. Wang, B. Jing, D. Xu, Y. Liao, H. Song, B. Sun, W. Gao, J. Xu, K. Li, M. Hu, S. Liu, J. Ling, Y. Kuang, T. Zhang, S. Zhang, F. Yao, B.P. Zhou, J. Deng, PTGES/PGE2 signaling links immunosuppression and lung metastasis in Gprc5a-knckout mouse model, Oncogene 39 (2020) 3179–3194.
[66] B.T. Kopp, R. Thompson, J. Kim, R. Konstan, A. Diaz, B. Smith, C. Shrestha, L. K. Rogers, D. Hayes, Jr, D. Tumin, F.W. Woodley, O. Ramilo, D.B. Sanders, J. A. Groner, A. Mejias, Secondhand smoke alters arachidonic acid metabolism and inflammation in infants and children with cystic fibrosis, Thorax 74 (2019) 237–246.
[67] T. Musso, P. Cappello, S. Stornello, D. Ravarino, C. Caorsi, K. Otero, F. Novelli, R. Badolato, M. Giovarelli, IL-10 enhances CCL2 release and chemotaxis induced by CCL16 in human monocytes.
[68] K. Kamio, A. Azuma, K. Matsuda, J. Usuki, M. Inomata, A. Morinaga, T. Kashiwada, N. Nishijima, S. Itakura, N. Kokuho, K. Atsumi, H. Hayashi, T. Yamaguchi, K. Fujita, Y. Saito, S. Abe, K. Kubota, A. Gemma, Resolution of bleomycine-induced pulmonary fibrosis via a splenic lymphocyte subpopulation, Respir. Res. 19 (2018) 71.
[69] S. Thavapalachandran, T.Y.L. Le, S. Romanazzo, F.N. Rashid, M. Ogawa, K. A. Kilian, P. Brown, J. Pouliopoulos, A.M. Barry, P. Fahmy, K. Kelly, E. Kizana, J.J. H. Chong, Pluripotent stem cell-derived mesenchymal stromal cells improve cardiac function and vascularity after myocardial infarction, Cytotherapy 23 (2021) 1074–1084.
[70] H. Yang, R. Feng, Q. Fu, S. Xu, X. Hao, Y. Qiu, T. Feng, Z. Zeng, M. Chen, S. Zhang, Human induced pluripotent stem cell-derived mesenchymal stem cells promote healing via TNF-alpha-stimulated gene-6 in inflammatory bowel disease models, Cell Death Dis. 10 (2019) 718.
[71] A.M. Foskett, N. Bazhanov, X. Ti, A. Tiblow, T.J. Bartosh, D.J. Prockop, Phase-directed therapy: TSG-6 targeted to early inflammation improves bleomycin-injured lungs, A, J. Physiol. Lung Cell. Mol. Physiol. 306 (2014) L120–L131.
[72] M.J. Chung, J.Y. Son, S. Park, S.S. Park, K. Hur, S.H. Lee, E.J. Lee, J.K. Park, I. H. Hong, T.H. Kim, K.S. Jeong, Mesenchymal stem cell and microRNA therapy of musculoskeletal diseases, Int. J. Stem Cells 14 (2021) 150–167.
[73] L.Y. Eun, H. Song, E. Choi, T.G. Lee, D.W. Moon, D. Hwang, K.H. Byun, J.H. Sul, K. C. Hwang, Implanted bone marrow-derived mesenchymal stem cells fail to metabolically stabilize or recover electromechanical function in infarcted hearts, Tissue Cell 43 (2011) 238–245.
[74] N.R. Danna, B.G. Beutel, K.A. Campbell, J.A. Bosco, 3rd, Therapeutic approaches to skeletal muscle repair and healing, Sports Health 6 (2014) 348–355.
[75] R. Xu, M. Wu, Y. Wang, C. Li, L. Zeng, Y. Wang, M. Xiao, X. Chen, S. Geng, P. Lai, X. Du, J. Weng, Mesenchymal stem cells reversibly de-differentiate myofibroblasts to fibroblast-like cells by inhibiting the TGF-beta-SMAD2/3 pathway, Mol. Med. 29 (2023) 59.
[76] A.J.C. Bloor, A. Patel, J.E. Griffin, M.H. Gilleece, R. Radia, D.T. Yeung, D. Drier, L. S. Larson, G.I. Uenishi, D. Hei, K. Kelly, I. Slukvin, J.E.J. Rasko, Production, safety and efficacy of iPSC-derived mesenchymal stromal cells in acute steroid-resistant graft versus host disease: a phase I, multicenter, open-label, dose-escalation study, Nat. Med. 26 (2020) 1720–1725.